1  # Extended calibration of cold-water coral Ba/Ca using multiple genera

2  # and co-located measurements of dissolved barium concentration

3  Peter T. Spooner[a,1,*], Laura F. Robinson[a], Freya Hemsing[b,c], Paul Morris[a,2], Joseph A.

4  Stewart[a]

5  [a]*School of Earth Sciences, University of Bristol, Queens Rd., Bristol, BS8 1RJ, UK*
6  [b]*School of Earth Sciences, University of Oxford, South Parks Rd., Oxford, OX1 3AN, UK*
7  [c]*Institute of Environmental Physics, Heidelberg University, Im Neuenheimer Feld 229, 69120*
8  *Heidelberg, Germany*

9  Abstract

10

11  Biological productivity and ocean circulation are both important oceanographic variables that

12  control the distribution of dissolved barium in the ocean interior ($[Ba]_{sw}$). The ability to

13  accurately reconstruct $[Ba]_{sw}$ will provide key constraints on these processes in the past. The

14  geochemistry of cold-water corals has the potential to unlock paleoceanographic records at

15  spatial and temporal resolutions not available using other sedimentary archives. Previous

16  studies have suggested that the Ba/Ca ratio of coral skeletons is linearly related to $[Ba]_{sw}$.

17  However, these efforts have used a limited number of species, sparse global seawater

18  databases, or have not explicitly measured the Ba/Ca ratio. Here we investigate the Ba/Ca

19  ratio in a well-constrained set of cold-water scleractinian (aragonitic) corals as a proxy for

20  $[Ba]_{sw}$, using 58 specimens from 7 coral genera along with co-located measurements of

21  $[Ba]_{sw}$. We find that traditional chemical cleaning procedures do not significantly affect the

22  Ba/Ca ratio of cold-water coral skeletons, allowing rapid sample throughput. We also

23  determine that intra-sample variation in Ba/Ca ratios can be reduced by using larger sample

24  sizes (e.g. 20 mg). By combining our results with existing data, we find that cold-water coral

25  Ba/Ca is linearly related to $[Ba]_{sw}$ according to the relationship: Ba/Ca µmol/mol = [0.15 ±

26  0.02] [$Ba_{sw}$ nmol/kg] + [2.5 ± 1.4], ($R^2$ = 0.7). We observe no species-specific 'vital effects' in

27  cold-water coral Ba/Ca ratios, but site-specific effects could be a factor. Nevertheless, our

28  results highlight the potential of Ba/Ca in cold-water corals to reconstruct biological and

29  physical changes in the ocean interior.

30

31

32

33  *Keywords:* Cold-water coral, Coral, Barium, Ba/Ca, Calibration

\* Corresponding author: p.spooner@ucl.ac.uk
[1]Present Address: Department of Geography, University College London, Gower Street, London, WC1E 6BT, UK
[2]Present Address: Department of Nuclear Sciences and Applications, International Atomic Energy Agency, Monaco

## 1. Introduction

The dissolved barium concentration in seawater ($[Ba]_{sw}$) has a nutrient-like profile (Chan et al., 1977; Jeandel et al., 1996). Depletions of $[Ba]_{sw}$ in the upper mixed layer are a result of adsorption/absorption of Ba onto organic particulates (Cardinal et al., 2005; Collier and Edmond, 1984; Hoppema et al., 2010; Jacquet et al., 2008, 2007; Sternberg et al., 2005). Ba is also removed from deeper waters (100-1000 m) as a result of barite formation in and around aggregates of sinking organic matter, and is released back into the water column following remineralisation (Bishop, 1988; Cardinal et al., 2005; Dehairs et al., 1980; Dymond et al., 1992; Ganeshram et al., 2003; Jacquet et al., 2007; Stroobants et al., 1991; van Beek et al., 2009). Collectively, these effects cause the deep ocean to be enriched in $[Ba]_{sw}$ relative to the surface. Therefore, knowledge of past dissolved barium concentration in the deep ocean may provide insight into paleo-ocean productivity and circulation.

Increasing attention is being paid to cold-water corals as paleoceanographic archives, with numerous elemental and isotopic ratios being tested as proxies for past ocean conditions (Robinson et al., 2014). Two key advantages of using scleractinian (aragonitic) corals for deep sea research are: 1) the ability to precisely date their skeletons using uranium (U)-series methods (Cheng et al., 2000), and 2) their wide geographic and bathymetric distribution, spanning multiple water masses and ocean basins (Roberts, 2006).

The Ba/Ca ratio in deep- and shallow-dwelling scleractinian coral skeletons (aragonite) has been shown to reflect the concentration of dissolved Ba in seawater ($[Ba]_{sw}$) (Anagnostou et al., 2011; Gonneea et al., 2017; Hemsing et al., 2018; LaVigne et al., 2016). This result is similar to findings for calcitic corals, foraminifera and inorganic aragonite (Dietzel et al., 2004; Hönisch et al., 2011; LaVigne et al., 2011; Lea and Boyle, 1993), and appears to be robust despite a range of vital effects that occur during coral growth (e.g. Adkins et al., 2003; Case et al., 2010; Gaetani and Cohen, 2006; Sinclair et al., 2006; Spooner et al., 2016b). These vital effects are often most apparent between two microstructures of the coral skeleton, centres of calcification (COCs) and fibrous aragonite thickening deposits (TDs) (Fig. 1). Yet, limited data suggest that, in cold-water corals, the Ba/Ca ratio is largely invariant between COCs and TDs (Anagnostou et al., 2011). Thus, whilst the relative proportions of these microstructures in a sample can hamper the use of many traditional paleoceanographic proxies such as Mg/Ca (Gagnon et al., 2007), the Ba/Ca ratio may be

70  less affected. However, several issues remain to be addressed to allow the use of Ba/Ca as

71  a tracer for past $[Ba]_{sw}$.

72

73  Previous studies have highlighted the impact of chemical cleaning on elemental ratios in

74  biogenic carbonates, results that may be ascribed to either removal of contaminants (such

75  as adsorbed metals, organics or Fe-Mn oxides) and/or partial skeletal dissolution during acid

76  leaching and reductive steps (Barker et al., 2003; Cheng et al., 2000; Mitsuguchi et al., 2001;

77  Montagna et al., 2014; Rosenthal et al., 2004; Shen and Boyle, 1988; van de Flierdt et al.,

78  2010; Watanabe et al., 2001). Studies have generally found no impact of cleaning on coral

79  Ba/Ca (Holcomb et al., 2015; Tudhope et al., 1996), but the subject warrants further testing

80  to develop a robust and reproducible methodology for cold-water corals.

81

82  Thus far, there has been no concerted study explicitly measuring Ba/Ca ratios in multiple

83  species of cold-water coral with dedicated measurements of $[Ba]_{sw}$, leaving questions as to

84  the impact of species- (or genus-) specific, and site-specific vital effects. Here we present a

85  new calibration of cold-water coral Ba/Ca versus $[Ba]_{sw}$ based on a recently-collected sample

86  set from the Atlantic and Southern Ocean (SO)(Chen et al., 2015; Spooner et al., 2016b).

87  Samples in this collection are precisely located and many were alive upon collection. We

88  present data from 58 individual specimens, representing 7 different coral genera from two

89  different ocean settings. We further improve on previous studies by calibrating the coral

90  Ba/Ca ratios against co-located $[Ba]_{sw}$ and by assessing the impacts of using different

91  cleaning procedures and sample sizes on cold-water coral Ba/Ca ratios. Furthermore, we

92  use measurements of other local seawater properties (temperature, salinity, nutrients,

93  oxygen concentration and carbonate chemistry) to assess the impact of these auxiliary

94  factors on the Ba-calibration and its potential paleoceanographic utility.

95

96

## 2. Methods

98

### 2.1. Coral sample collection and dating

100

101  Coral skeletons were collected during three cruises (NBP0805, NBP1103 and LMG0605) to

102  the SO (Drake Passage), one cruise (JC094) to the tropical Atlantic Ocean (Fig. 2), and one

103  cruise to the Reykjanes Ridge (CE0806) (Burke and Robinson, 2012; Chen et al., 2015;

104  Jones et al., 2014; Spooner et al., 2016b). Note that samples from the Reykjanes Ridge

105  were only included in the cleaning and sample-size experiments (Section 2.4) and not the

106  calibration because of a lack of $[Ba]_{sw}$ at the depths of the samples in this study. Samples for

the calibration were either collected alive using a Remotely Operated Vehicle (ROV, tropical Atlantic samples, n = 33) or were sub-fossil specimens (i.e. dead) with skeletons <1 ka old, collected using dredges and trawls (Drake Passage samples, n = 25). The majority of dead sample ages were determined via U-series isotope dilution solution multi-collector inductively-coupled plasma mass spectrometry (MC-ICPMS) (Burke and Robinson, 2012) and the remainder by reconnaissance radiocarbon/U-series dating (Burke et al., 2010; Burke and Robinson, 2012; Margolin et al., 2014; Spooner et al., 2016a) (Table S1).

Sample depths ranged from 210 to 2500 m (Table S1). Sample locations using dredges and trawls are listed as the mean depth, latitude and longitude for each collection event. Drake Passage genera included *Balanophyllia*, *Caryophyllia*, *Desmophyllum* and *Flabellum*. Tropical Atlantic genera included *Caryophyllia*, *Dasmosmilia*, *Enallopsammia* and *Javania*. With the exception of *Enallopsammia* (a colonial coral), these are all solitary, scleractinian (aragonitic) corals (a single coral polyp with its own skeleton, typical morphological features shown in Fig. 1) (Cairns and Kitahara, 2012). Thus far, *Desmophyllum dianthus* has been the most commonly used solitary cold-water solitary coral in paleoceanographic studies (e.g. Burke and Robinson, 2012; Thiagarajan et al., 2014). It has an attached base but lacks a columella or pali (Fig. 1). Corals from the genera *Javania* and *Flabellum* also have these characteristics, but *Javania* has a pedicel thickened with successive layers of aragonite. *Dasmosmilia* is also attached and has a rudimentary columella. *Balanophyllia* corals have a highly porous outer thecal layer, which often becomes infilled by secondary carbonate minerals. The polyps of the colonial coral *Enallopsammia* tend to be small, housed within a branching porous skeleton.

### 2.2. Dissolved Ba and other seawater properties

Water samples collected during the tropical Atlantic JC094 cruise have been analysed for $[Ba]_{sw}$ previously (Bates et al., 2017). These water samples were from three locations across the Atlantic: Carter Seamount (JC094-CTD002), Vema Fracture (JC094-CTD005) Zone and Vayda Seamount (JC094-CTD006) (Fig. 3). These three sites had very similar $[Ba]_{sw}$ profiles suggesting that they are representative of the tropical Atlantic region. We therefore used these profiles to estimate $[Ba]_{sw}$ for the remaining tropical Atlantic sample sites (Fig. 1).

Water collected during the Drake Passage NBP1103 cruise was analysed for $[Ba]_{sw}$ at the University of Oxford as part of a companion study on barium isotopes (Hemsing et al., 2018).

143 Samples were taken from Burdwood Bank (NBP1103-CTD021) and Sars Seamount
144 (NBP1103-CTD100) (Fig. 2 and 3).

145

146 Temperature (T) and salinity (S) (Fig. 3; Table S2) were measured at or near each coral
147 collection site and compared with ocean atlas data (Levitus and Boyer, 1994) to estimate the
148 variability of these parameters at each sample site, following the methods in Spooner et al.
149 (2016b).

150

151 For cruise JC094, major nutrients (nitrate, phosphate, silicic acid; Table S2) were measured
152 at the University of Plymouth in seawater samples frozen at -20 $^{o}$C during the cruise (Bates
153 et al., 2017; Robinson, 2014). During the Southern Ocean cruises, filtered seawater samples
154 were also frozen at -20 $^{o}$C before nutrient concentrations were measured at Woods Hole
155 Oceanographic Institution Nutrient Analytical Facility (e.g. Hendry et al., 2010).

156

157 During NBP0805 and NBP1103, dissolved oxygen concentrations (ml/l) were measured with
158 a Sea-Bird Electronics-43 dissolved oxygen sensor attached to the CTD carousel. Data were
159 converted to µmol/l based on the standard conversion used in the Sea-Bird Electronics
160 software. During JC094, dissolved oxygen concentration was also measured using a Sea-
161 Bird Electronics-43 sensor. Shipboard measurements were also performed on every water
162 sample using Winkler titrations to ensure a good sample calibration of the Sea-Bird sensor
163 (Carritt and Carpenter, 1966; Robinson, 2014).

164

165 Carbonate chemistry parameters (total alkalinity and dissolved inorganic carbon) for the
166 tropical Atlantic sites were measured by the UK Ocean Acidification Research Program
167 Carbonate Chemistry Facility at the National Oceanography Centre (NOC), Southampton, in
168 seawater samples that were collected close to the coral collection sites (Robinson, 2014).
169 For the Southern Ocean sites we made use of a recent carbonate system re-analysis to
170 estimate the parameters of interest (Bostock et al., 2013). We used estimates of the
171 alkalinity and dissolved inorganic carbon from the re-analysis at the grid location and depth
172 closest to each sample site and the measured temperature, salinity and nutrient data from
173 each site (measured during the sample collection cruises) to estimate the remaining
174 carbonate system parameters using the CO2SYS program (Pierrot et al., 2006).

175

176 Water sampling was typically carried out at ~12 depths per location. Therefore, we linearly
177 extrapolated measurements from the depths closest to coral collection sites to estimate the
178 water properties at those depths (Table S2).

179

### 2.3. Sample preparation

Immediately after collection from the seabed, sub-fossil (i.e. dead) coral skeletons were rinsed with fresh water. Live-collected corals were bleached to remove external organic tissue, followed by freshwater rinses of the skeletons. All skeletons were then dried at room temperature. Approximately 20 mg of each coral was cut using a hand-held diamond saw. Samples were generally cut from the upper portion of the skeleton and included portions of both thecal and septal material (Fig. 1, Table S1). Relative proportions of COCs and TDs were not monitored. For the genus *Enallopsammia*, samples were taken from both the tips of branches (i.e. polyp material) or the branches themselves. Each subsample was physically cleaned by gently milling the surfaces with the flat of the diamond saw to remove visible ferro-manganese crusts (for some sub-fossil specimens) and/or altered/chalky carbonate, or possible organic residues on live-collected specimens. The porous outer skeleton of all *Balanophyllia* corals was removed as much as possible. Samples were then ultrasonicated (US) in 18.2 MΩcm water (MQ) for 15 minutes to remove particulates introduced during the cutting and milling, rinsed with MQ and dried at room temperature.

Dry coral samples were placed in acid-cleaned Teflon vials for storage and dissolution. On the day of analysis, samples were dissolved in 50 μl concentrated super-pure (s.p.) $HNO_3$ and then diluted with 1.95 ml 0.5 M s.p. $HNO_3$. In preparation for ICPMS measurement, aliquots of each sample were further diluted into acid-cleaned Teflon autosampler vials to obtain solutions with Ca concentrations ([Ca]) of ~2.5 mM, in 1.5 ml of 0.5 M s.p. $HNO_3$. Dilutions were doped to 4 ppb In. Full procedural blanks were prepared in the same way as the samples.

### 2.4. Cleaning and sample size experiments

Cleaning tests were carried out on large aliquots of 15-20 mg taken from two powdered samples of sub-fossil coral. One sample (CE0806-Dr-18-1, Reykjanes Ridge) was ~110 ka old with an extensive, black ferro-manganese crust (Spooner et al., 2016a). The other sample (NBP1103-TB10-Dp-3, Drake Passage) was <1 ka old and lacked such crusts.

We used standard cleaning procedures designed to remove adsorbed metals, ferro-manganese crusts and organic material, adapted from procedures used during U-series and trace metal analysis of cold-water corals (Burke and Robinson, 2012; Cheng et al., 2000;

Shen and Boyle, 1988). The cleaning steps (each followed by three MQ water rinses) were as follows, with: Every coral underwent shipboard freshwater rinses, followed by lab-based removal of ferro-manganese crusts and visibly altered aragonite with a diamond disc. This physical clean was followed by 15 min ultrasonication (US) in MQ to remove adsorbed metals and other contaminants introduced during sample preparation and step 1 (Mitsuguchi et al., 2001). After this step, large pieces of coral aragonite were cut and powdered in a pestle and mortar for further cleaning, and different aliquots of the powder were then rinsed with MQ and subjected to between none and all of the following chemical cleaning steps: 1) 15 min US in an oxidising, 1:1 mixture of 30 % $H_2O_2$ and 1 M NaOH, heated to ~60 $^o$C to remove organics; 2) 2 min rinse in a 1:1 mixture of 1 % $HClO_4$ and 30 % $H_2O_2$, to vigorously remove remaining organics (Cheng et al., 2000); 3) step 2 repeat; 4) 1 min US in 0.2 % (by mass) $HNO_3$, to leach remaining surficial contaminants; 5) step 3 repeat; 8) 20 min US in a reducing solution, made by mixing 20 ml of solution A (see below) with 20 ml $NH_4OH$ (conc.) and 1.5 ml hydrazine, to remove remaining metal-rich oxides. Solution (A) was made by dissolving 30 g citric acid powder into 250 ml of milli-q and adding 250 µl $NH_4OH$ (conc.).

In addition to the effects of cleaning, it is possible that intra-skeletal variability could result in scatter in a Ba/Ca versus $[Ba]_{sw}$ calibration. Therefore, we carried out two experiments to test the effect of sample size on measurement reproducibility. The coral NBP0805-TB04-Big Beauty was collected from the Drake Passage and is included in the calibration study. Ten solid subsamples were cut each of 5 mg, 10 mg, 20 mg and 40 mg. The coral CE0806-Dr04A-1 was collected during a cruise to the Reykjanes Ridge, Iceland (CE0806). For this coral, five subsamples were taken each of 5 mg, 10 mg, 20 mg and 40 mg. Samples were prepared as described above but were not chemically cleaned given the results of the cleaning experiments (Section 3.1). Ba/Ca was measured in each sample as described below and the reproducibility calculated for each size class.

## 2.5. Measurement procedures

A multi-element standard (CrlME) containing Li, B, Mg, P, Ca, Fe, Mn, Sr, Ba and U was gravimetrically prepared by mixing single-element solutions supplied by High-Purity Standards Incorporated. CrlME element/Ca ratios were calculated based on the mass, density, elemental concentration (in µg $l^{-1}$) and impurity data (supplied with the certification for each solution) of each single element solution, and were designed to reflect average cold-water scleractinian coral values found in the literature (final gravimetric Ba/Ca = 7.64 ±0.05 µmol/mol). On the day of analysis, the standard was diluted into sample vials to a concentration of ~2.5 mM Ca.

Samples were measured in the Bristol Isotope Group (BIG) using a ThermoFinnigan Element 2 ICPMS following standard methods (e.g. Rae et al., 2011; Rosenthal et al., 1999). Prior to running full trace metal analysis, sample Ca concentrations ([Ca]) were checked by comparison with four solutions of varying [Ca] (0.5 mM, 1 mM, 2.5 mM and 5 mM). If necessary, samples were re-diluted to ensure that their [Ca] was within 10 % of the multi-element standard (typically ~2.5 mM [Ca]). The majority of the samples were matched to the [Ca] of the CrlME standard to within 2 %.

During sample analysis $^{43}$Ca, $^{48}$Ca, $^{115}$In and $^{137}$Ba were measured in low resolution. $^{55}$Mn, $^{56}$Fe and $^{115}$In were measured in medium resolution. $^{115}$In was used to normalise the medium resolution measurements to obtain Mn/Ca and Fe/Ca. Each sample acquisition took 3.5 minutes. CrlME was run at the start and end of the sequence and after every two samples, and was used to calculate elemental ratios (El/Ca$_{sample}$) from counts per second data using the approach of (Rosenthal et al., 1999).

Procedural blanks were measured before and after each standard measurement, the averages of which were subtracted from measured standard/sample signal intensities before calculation of elemental ratios. Typical blank intensities were 0.1 % for $^{137}$Ba and 0.01 % for $^{43}$Ca and $^{48}$Ca.

Element/calcium ratios were calculated using both $^{43}$Ca and $^{48}$Ca, and the results were compared for each sample run. There was no significant difference between these two calculation methods for any of the samples. Reported elemental ratios (Table S1) are the mean of the ratios calculated using $^{43}$Ca and $^{48}$Ca.

Fe/Ca and Mn/Ca measurements were used to assess potential contamination from residual ferro-manganese crusts not removed by physical cleaning.

Three consistency standards were used to determine measurement accuracy and precision: 1) the coral powder JCp-1 (Okai et al., 2002); 2) an in-house cold-water coral powder (Dr18-1p) and 3) a second multi-element solution (PTS-1), prepared similarly to CrlME. JCp-1 has been the subject of an interlaboratory calibration exercise for elemental ratios (Hathorne et al., 2013). The mean Ba/Ca value measured for JCp-1 in this study (6.96 ± 0.08 µmol/mol 2 S.E., n = 13) was less than the average value of 7.465 ± 0.655 µmol/mol in Hathorne et al. (2013), but the results are within the robust interlaboratory 2 S.D. We also measured Ba/Ca in an in-house mixed solution standard BSGS (Ni et al., 2007; Rae et al., 2011). The Ba/Ca

291 ratio we measured was within 2 % of those studies. To facilitate comparison with Hemsing et

292 al. (2018) (who measured Ba/Ca of JCp-1 = 7.94 ± 0.22 µmol/mol), we here adjust our

293 respective data sets by factors required to obtain JCp-1 Ba/Ca = 7.465 µmol/mol (i.e. x1.073

294 in this study, and x0.940 for data from Hemsing et al. (2018)).

295

296 Based on measurements of PTS-1 (83 measurements) and Dr18-1p (12 measurements), the

297 12-month Ba/Ca reproducibility was ± 1.6 % 2 standard deviations (2 S.D.).

298

299

300 ## 3. Results

301

302 ### 3.1. Cleaning experiments and Fe/Ca

303

304 The maximum difference in Ba/Ca between powder aliquots cleaned to different extents was

305 2.6 % (Fig. 4, Table 1). NBP1103-TB10-Dp-3 did not show any consistent change in Ba/Ca

306 with progressive cleaning. However, the Ba/Ca ratio in CE0806-Dr18-1 decreased by 2.6 %

307 after the oxidative/perchloric acid steps. This difference in results for the two corals may be

308 due to relatively high Fe/Ca ratios in CE0806-Dr18-1, possibly indicating contamination by

309 non-carbonate phases (e.g. ferro-manganese oxides) that were removed during the

310 oxidative cleaning (Cheng et al., 2000). The two aliquots limited to physical cleaning and

311 water washes had Ba/Ca ratios of 6.83-6.85 µmol/mol and Fe/Ca ratios of 40-50 µmol/mol.

312 After cleaning with oxidising solution and perchloric acid, Ba/Ca ratios fell to 6.70 µmol/mol

313 and Fe/Ca ratios fell to <20 µmol/mol.

314

315 In agreement with other studies, our cleaning results for these corals show that, even in the

316 presence of relatively high Fe concentration (i.e. potentially high volumes of contaminating

317 phases), the effect of chemical cleaning on coral Ba/Ca is small (Holcomb et al., 2015). It

318 has also been shown that such chemical cleaning can lead to selective dissolution of

319 carbonate material (e.g. Barker et al., 2003), which could have inconsistent impacts on

320 measured skeletal geochemistry.. We therefore did not  clean samples used for the

321 calibration beyond the basic mechanical cleaning. In order to account for the potential impact

322 of contaminating phases outlined above, we use Fe/Ca ratios to exclude potentially

323 contaminated samples from the analyses.

324

325 A common limit applied to foraminifera to exclude contaminated carbonate is that Fe/Ca

326 should be <175 µmol/mol (e.g. Bice et al., 2005; Lea et al., 2005). However, given the

327 results outlined above we take a conservative approach to identifying contamination by

328  excluding samples with Fe/Ca >40 µmol/mol from the analyses. Two measurements were

329  excluded in this way (Table S1). The mean Fe/Ca ratio of all samples with Fe/Ca <40

330  µmol/mol was 3 µmol/mol.

331

### 3.2. Sample size experiments

333

334  In both corals analysed for different size samples, the reproducibility of Ba/Ca (2 S.D.) was

335  better than 10 % for all size categories and generally improved with increasing sample size

336  (Fig. 5). For the 20 mg category, reproducibility was 7 % for NBP0805-TB04-Big Beauty and

337  6 % for CE0806-Dr04A-1. These values are greater than the variability in the cleaning

338  experiments because subsamples were distinct (i.e. not powdered and mixed) and represent

339  different areas of the skeleton. Based on the results of this experiment, we chose used 20

340  mg samples from each coral in the calibration as a compromise between reproducibility and

341  sample limitation in smaller specimens. Such samples are large compared to previous work

342  (e.g. laser ablation) and given our results may be expected to decrease scatter in the

343  calibration. Using these methods, our data suggest that intra-skeletal variability could

344  introduce scatter of ~7 % into the Ba/Ca values.

345

### 3.3. Calibration of cold-water coral Ba/Ca versus [Ba]$_{sw}$

347

348  We find that coral Ba/Ca is linearly related to [Ba]$_{sw}$ (Fig. 6). After adjustment by the factor

349  required to bring our JCp-1 data into agreement with Hathorne et al. 2013 (i.e. x1.073), a

350  linear least squares regression of the coral measurements (average for each specimen) in

351  this study suggests the calibration equation: Ba/Ca µmol/mol = [0.12 ± 0.02] [Ba$_{sw}$ nmol/kg] +

352  [4.72 ± 1.08], $R^2$ = 0.79, p < 0.01. The regression results in prediction errors (uncertainty of

353  predicting [Ba]$_{sw}$ based measured Ba/Ca in corals) of ~14- nmol/kg (95 % confidence) (Fig.

354  7). Regressing the same data using a weighted bivariate regression approach (Cantrell,

355  2008; York et al., 2004), results in a slightly steeper slope and lower intercept than obtained

356  using the standard least squares fit: Ba/Ca µmol/mol = [0.15 ± 0.02] [Ba$_{sw}$ nmol/kg] + [2.86 ±

357  1.09], with a goodness of fit parameter equal to 2.8 (Cantrell, 2008), indicating that the

358  model has not fully captured the data variability. The regression models  suggest that the

359  standard least squares fit likely represents a minimum of the Ba/Ca versus [Ba]$_{sw}$ slope and

360  is therefore the more conservative choice for interpreting paleo data. We also note that the

361  lines are within uncertainty of one another and do little to change the data interpretation

362  here. Hence, for simplicity, discussion (below) is based on the least squares calibration. We

363  note that, even without standard-based adjustment of the data, the calibration has a

364  significantly positive y-intercept.

Residuals are consistent with a normal distribution according to a Kolmogorov-Smirnov (K-S) test for normality. Residuals are not related to $[Ba]_{sw}$, suggesting that a linear fit to the data is appropriate for the data range covered. The numbers of samples from individual genera are small (3 to 20), but further genus-specific K-S normality tests indicate that the residuals for each coral genus are consistent with normal distributions. Applying t-tests to the residuals of these genera indicates that no genus has a mean residual that is significantly different to that of any other genus, suggesting that genus-specific vital effects are not important for skeletal Ba/Ca ratios.

## 4. Discussion

### 4.1. Covariance of seawater properties

Our coral data indicates that $[Ba]_{sw}$ can explain 79 % of the variance in coral Ba/Ca. The residuals of the regression are not significantly correlated with temperature, salinity, carbonate ion concentration, nutrient concentration or oxygen concentration. For corals living within the thermocline (tropical Atlantic *Dasmosmilia*), it is possible that seawater properties changed over the lifetime of the corals. However, we largely discount this factor as a dominant driver of coral Ba/Ca scatter, as similar variability occurs in samples from the same locations and depths, suggesting that the residual spread of data is more likely to be explained by intra-skeletal variability in the Ba/Ca ratio.

Superficially, coral Ba/Ca appears to be related to in-situ T and S (Fig. 8). However, these relationships are clearly dominated by the covariation between $[Ba]_{sw}$, T and S in the water column. For example, while coral Ba/Ca and T appear correlated in Figure 8b, the correlation is not linear. Rather, the Ba/Ca ratios of Drake Passage corals change more rapidly with T than those from the tropical Atlantic. This pattern closely matches the relationship between $[Ba]_{sw}$ and T across the sites (Fig. 8a), indicating that the correlation between Ba/Ca and T is driven by the dependence of Ba/Ca on $[Ba]_{sw}$. The same argument can be made for the correlation between Ba/Ca and salinity (Figures 8c and 8d).

These inferences are supported by a recent culturing study that found strong dependence of warm-water coral Ba/Ca on $[Ba]_{sw}$, and relatively minor T dependence (Gonneea et al.,

2017). However, the results of this culturing study and other experimental studies of abiogenic aragonite growth reveal that low temperatures are associated with higher aragonite Ba/Ca ratios, showing that temperature does have some effect on coral Ba/Ca ratios (Dietzel et al., 2004; Gaetani and Cohen, 2006). Because the corals from our study from areas with high $[Ba]_{sw}$ (Drake Passage) were also living in low temperature environments, the temperature effect described above would increase the slope of our calibration. Based the results of Gonneea et al. (2017) and Dietzel et al. (2004) and assuming a low-end partition coefficient between aragonite and seawater of 1.5 ($D_{Ba/Ca}$, Section 4.4), the 8 $^{\circ}$C temperature increase across our sites would result in a small but measurable 1 µmol/mol decrease in coral Ba/Ca. This could account for around 14 % of the total change in Ba/Ca, with the rest attributed to changes in $[Ba]_{sw}$. However, both of the experiments cited above were conducted at temperatures above those experienced by our coral samples (10 – 50 $^{\circ}$C), and disagree in the magnitude of the temperature effect with another study conducted at even higher temperature (Gaetani and Cohen, 2006), highlighting the need for further controlled experiments to assess the impact of temperature on Ba/Ca, particularly in cold-water specimens.

### 4.2. Comparison to existing $[Ba]_{sw}$ calibrations

The cold-water coral Ba/Ca versus $[Ba]_{sw}$ calibration using data from this study suggests a well-defined, linear relationship, despite the inclusion of samples from different sites and coral genera. However, there remain some discrepancies between these new calibration data and those presented in other studies (Fig. 9).

In a study on barium isotopes (Hemsing et al., 2018), Ba/Ca ratios were obtained as an ancillary product in a sample set that included the major sample locations in this study, and also Iceland (Fig. 9). A total of 15 coral specimens (different subsamples) were measured by both studies. After adjusting the data each study by the factors outlined in Section 2.5, the Ba/Ca ratios of these 15 shared samples do not differ by more than 10 % between the studies, in line with the expected intra-skeletal variability found in our sample size experiments.

Combined (with averages taken for replicate samples), the data from the two studies suggest the relationship: Ba/Ca µmol/mol = [0.15 ± 0.02] [$Ba_{sw}$ nmol/kg] + [2.5 ± 1.4], $R^2$ = 0.70, p < 0.01 (Fig. 9). This relationship has a higher slope and lower intercept than found with the corals measured only in this study. However, the Ba/Ca ratios for corals from the same sample sites agree very well between the two studies (Fig. 9). The discrepancy

439 between the regression models arises because every sample from Iceland (Hemsing et al.
440 2018) has relatively low Ba/Ca compared to corals from the other sites with similar $[Ba]_{sw}$,
441 even though they represent a mixture of three different species (Fig. 9). This finding
442 suggests that there could be a site-specific effect acting on these corals (Section 4.3).

443

444 The only other study to examine Ba/Ca in cold-water corals used laser ablation analyses in a
445 sample set mainly based on museum specimens (Anagnostou et al., 2011). The laser
446 ablation was used to target TDs in *D. dianthus*. This study found the relation: Ba/Ca
447 µmol/mol = [0.09 ± 0.05] [$Ba_{sw}$ nmol/kg] + [2.9 ± 3.4]. The scatter in this data set is relatively
448 large (i.e. a zero or non-zero intercept cannot be established), with some of the corals falling
449 close to our calibration, while other Ba/Ca ratios plotting up to 4 µmol/mol below (Fig. 9). The
450 relatively low and scattered laser ablation Ba/Ca results may stem from analytical artefacts,
451 uncertainty in $[Ba]_{sw}$, site-specific effects (as above), or micro-structure coral heterogeneities.
452 We consider the first of these reasons to be the main factor. Although estimates of $[Ba]_{sw}$
453 were not taken from co-located seawater measurements (as in our current study),
454 uncertainties beyond 10 nmol/kg seem unlikely. Samples were collected from a wider variety
455 of sampling sites (Atlantic, Pacific, Southern Ocean), so that low Ba/Ca ratios cannot be
456 ascribed to any particular location. In addition, the Ba/Ca of samples from Burdwood Bank at
457 ~400 m depth that we measure (~12 µmol/mol) is 40 % higher than the Ba/Ca measured in a
458 similar sample by Anagnostou et al., (2011) (8.48 µmol/mol), suggesting that effects other
459 than sample site-specific effects are affecting the data. In the one coral sample where both
460 COCs and fibrous aragonite TDs were targeted by laser work, it was suggested that these
461 microstructures do not have very different Ba/Ca ratios (Anagnostou et al., 2011), although
462 micron-scale heterogeneities cannot be completely ruled out. While laser-ablation
463 techniques offer elemental mapping capabilities at unprecedented spatial resolution, there
464 are clear analytical draw-backs to this approach in the form of variable matrix effects and a
465 lack of suitably homogenous, well-characterised, LA-ICP-MS carbonate reference material to
466 permit direct data comparison between laboratories (Limbeck et al., 2015). Thus, while the
467 results of Anagnostou et al. (2011) represent an important first step towards ground-truthing
468 the proxy and in general support the proposed sensitivity (slope) of coral Ba/Ca to $[Ba]_{sw}$ in
469 our study, we likely cannot directly compare absolute values between the two studies.

470

471 Ba/Ca measurements in the warm-water scleractinian corals *Porites lobata*, *Pavona*
472 *gigantea* and *Pavona clavus* were compared to $[Ba]_{sw}$ measured over the course of a year in
473 the Gulf of Panama (LaVigne et al., 2016). Taking these data together they give the
474 relationship: Ba/Ca µmol/mol = [0.99 ± 0.02] [$Ba_{sw}$ nmol/kg] + [1.0 ± 1.2]. In a recent study,
475 Ba/Ca was measured in cultured specimens of the warm-water scleractinian *Favia fragum* at

476 three different temperatures (Gonneea et al., 2017). Without forcing the regression line

477 through the origin, data from three corals grown at 27.7 $^{\circ}$C suggest a calibration line of:

478 Ba/Ca μmol/mol = [0.17 ± 0.004] [Ba$_{sw}$ nmol/kg] - [1.0 ± 1.0].

480 With respect to the cold-water calibrations we present here, the corals from LaVigne et al.

481 (2016) show a similar Ba/Ca sensitivity to [Ba]$_{sw}$, but all have Ba/Ca values that are around 4

482 μmol/mol lower for similar [Ba]$_{sw}$. Based on the temperature effect discussed above, around

483 2 μmol/mol of this difference could be explained by the relatively warmer temperatures

484 experienced by these tropical corals. However, despite also being grown in warm water, the

485 Ba/Ca value of the cultured warm-water coral *Favia fragum* specimen grown at [Ba]$_{sw}$ of 79 ±

486 23 nmol/kg is closer to that which would be expected from our calibration (Gonneea et al.,

487 2017), again pointing to the need for more culturing experiments to better define the culture

488 calibration at natural [Ba]$_{sw}$ concentrations, to determine whether there is some difference in

489 Ba uptake by warm- and cold-water corals or non-linearity in the calibration at extremely low

490 [Ba]$_{sw}$ values.

### 492 4.3. Genus- and site-specific calibrations

494 As well as potential bias in the calibration related to temperature change, additional Ba/Ca

495 variability may stem from genus- and/or site-specific effects. Indeed, we have shown above

496 that the combined calibration between this study and Hemsing et al. (2018) reveals a

497 potential site-specific effect observed in the Icelandic corals.

499 Species-specific effects may arise because of differences in coral physiology or calcification

500 (e.g. Spooner et al., 2016b). However, a standard linear least squares calibration based only

501 on *Caryophyllia*, the genus with the most samples (n = 24, including Hemsing et al. 2018)

502 and greatest range in [Ba]$_{sw}$ (~50 nmol/kg) returns a line statistically identical to the overall

503 regression: Ba/Ca$_{Caryophyllia}$ μmol/mol = [0.13 ± 0.03] [Ba$_{sw}$ nmol/kg] + [3.6 ± 1.8], R$^2$ = 0.79, p

504 < 0.01. This result, combined with the genus-specific residuals detailed in Section 3.3,

505 suggests that genus/species-specific effects are minor and that the calibration may be

506 applicable to all cold-water scleractinia.

508 However, the possibility of site-specific effects on coral Ba/Ca complicates this picture.

509 Unfortunately, the small range in [Ba]$_{sw}$ experienced by the Icelandic samples precludes

510 defining a calibration line for that site. Combining the data from this study and from Hemsing

511 et al. (2018) (as above, i.e. averaging data for replicated samples) and excluding the Iceland

512 samples, we obtain the relationship: Ba/Ca μmol/mol = [0.12 ± 0.02] [Ba$_{sw}$ nmol/kg] + [4.4 ±

513    1.0], $R^2$ = 0.78, p < 0.01, statistically the same as that using only the data in this study.

514    Samples from the tropical Atlantic give the regression line: Ba/Ca μmol/mol = [0.085 ± 0.04]

515    [$Ba_{sw}$ nmol/kg] + [6.3 ± 2.3], $R^2$ = 0.28, p < 0.01. The slope and intercept of this line are

516    within error of those for the overall regression, but the line is naturally more poorly fit due to

517    the small range in [Ba]$_{sw}$ of ~25 nmol/kg. This relationship also represents all the data for

518    live-collected specimens, indicating that the overall result is robust with or without inclusion

519    of sub-fossil material. A regression through the Southern Ocean samples gives a similar

520    regression over a wider range of [Ba]$_{sw}$: Ba/Ca μmol/mol = [0.10 ± 0.03] [$Ba_{sw}$ nmol/kg] +

521    [6.54 ± 2.12], $R^2$ = 0.68, p < 0.01. The similarity of both of these lines with the overall

522    regression again suggests that the results from Iceland are anomalous.

523

524    Cooler temperatures in Icelandic waters would serve to slightly increase coral Ba/Ca relative

525    to low latitude sites. Therefore, a temperature effect alone cannot explain the low Icelandic

526    Ba/Ca values. It could be that the measurements of [Ba]$_{sw}$ for the Iceland sites, taken in

527    June, are not representative of the annual value, due to either substantial seasonal changes

528    in export productivity or to the seasonal strength of Iceland-Scotland Overflow Water (Bower

529    and Furey, 2017; Sundby et al., 2016). A further possibility is that the conditions for coral

530    growth around Iceland impact coral calcification in other ways, perhaps by affecting growth

531    rates or the relative proportions of different skeletal microstructures. These ideas are

532    speculative and new measurement campaigns on other sample sites will be needed to

533    explore the possibility of site-specific vital effects further.

534

535

536    ### 4.4.  $D_{Ba/Ca}$

537

538    The distribution coefficient $D_{Ba/Ca}$ for coral aragonite is the ratio of Ba/Ca in the aragonite

539    structure to that of the water from which the aragonite precipitated: $D_{Ba/Ca}$ = (Ba/Ca$_{coral}$) /

540    (Ba/Ca$_{water}$). $D_{Ba/Ca}$ >1 indicates that Ba is preferentially incorporated into the aragonite (as

541    opposed to remaining in the water). To calculate $D_{Ba/Ca}$ for each coral here we make several

542    assumptions. We must assume that the corals are: 1) calcifying from a fluid of seawater

543    composition; 2) calcifying in an open system or else in a batch process in which the whole of

544    each batch of fluid is used up; and 3) that the only source of Ba to the skeleton is from the

545    seawater dissolved pool (i.e. if [Ba]$_{sw}$ = 0 then the coral skeleton Ba/Ca ratio would also be

546    zero). We take a constant value for seawater calcium concentration of 1.03  mmol/kg

547    (Nozaki, 1997), but given a salinity variation across our sample sites, we assume a 5 %

548    uncertainty on this value.

549

550 Under these assumptions we calculate $D_{Ba/Ca}$ values between 1.5 and 2.8 (Fig. 10).
551 However, the significantly positive y-intercept of our calibration (Section 3.3) shows that,
552 either $D_{Ba/Ca}$ changes systematically across the sample set (Fig. 10), or that one or more of
553 our assumptions are incorrect.

554

555 Our assumptions may be incorrect for several reasons. Firstly, the assumption that the
556 calcification fluid is of purely seawater composition is likely invalid. The favoured model of
557 coral calcification suggests that corals import $Ca^{2+}$ ions into the fluid (thus changing Ba/Ca)
558 at the expense of $H^+$ ions, in order to up-regulate the pH to the extent required to easily
559 precipitate aragonite (e.g. Cohen and McConnaughey, 2003; McConnaughey, 1989).
560 Secondly, the enclosed nature of the fluid likely precludes fully open-system behaviour,
561 allowing batch fractionation processes to affect skeletal chemistry on microscales that would
562 not be detectable using our bulk sampling methods (e.g. Case et al., 2010; Gaetani et al.,
563 2011; Montagna et al., 2014). Thirdly, while not yet demonstrated for cold-water corals, the
564 presence of Ba-rich, cleaning-resistant contaminating phases such as interstitial organics or
565 barite has been suggested for some warm-water corals (Tudhope et al., 1996). Although we
566 showed above that chemical cleaning has little effect on coral Ba/Ca ratios, it is unclear
567 whether such phases would have been completely removed by our cleaning experiments.

568

569 Given these issues with calculation of $D_{Ba}$ and the positive intercept of our calibration lines,
570 calculating past $[Ba]_{sw}$ from cold-water coral Ba/Ca using any single estimate of $D_{Ba}$ is not an
571 appropriate approach. However, the empirical calibration model of Ba/Ca vs $[Ba]_{sw}$
572 suggested by our data appears to be robust, despite inclusion of different species and
573 methodologies, and can therefore be used to estimate past $[Ba]_{sw}$.

574

575

576

577

578

579 **5. Conclusions**

580

581 We have investigated the applicability of the Ba/Ca proxy in cold-water corals for
582 determining the concentration of dissolved barium in seawater ($[Ba]_{sw}$) using solution-based
583 single collector inductively coupled plasma mass spectrometry. Combined with data from a
584 companion study, coral Ba/Ca appears to be linearly related to $[Ba]_{sw}$ according to the
585 relation: Ba/Ca µmol/mol = [0.15 ± 0.02] [$Ba_{sw}$ nmol/kg] + [2.5 ± 1.4].

586

587 A lack of correlation of the residuals of the regression with other ocean variables and the
588 minor effect of temperature suggest that $[Ba]_{sw}$ is the dominant driver of cold-water coral
589 Ba/Ca, explaining up to 79 % of the variance. The slope of this relationship is the same as
590 those found for warm-water corals in previous studies. However, for samples growing in
591 waters with low $[Ba]_{sw}$ (< 70 nmol/kg), cold-water corals appear to have higher Ba/Ca ratios
592 than their warm-water counterparts, by an amount that is greater than the expected effect of
593 temperature alone. In addition, we find that sample site-specific effects may be important for
594 cold-water coral Ba/Ca ratios, with samples from Iceland having consistently lower Ba/Ca
595 ratios than those from the tropical Atlantic.

596

597

598 Our calibration data from a variety of sample sites and genera imply that Ba/Ca
599 measurements in cold-water scleractinian corals can be used to reconstruct $[Ba]_{sw}$ in the
600 past ocean. Cold-water coral Ba/Ca is therefore a promising addition in the
601 paleoceanographer's tool kit that will provide constraints on productivity and ocean
602 circulation in the past.

603

604

605

618

### 7. References

620 Adkins, J.F., Boyle, E.A., Curry, W.B., Lutringer, A., 2003. Stable isotopes in deep-sea
621     corals and a new mechanism for "vital effects." Geochim. Cosmochim. Acta 67, 1129–

622    1143. https://doi.org/10.1016/S0016-7037(00)01203-6

623    Anagnostou, E., Sherrell, R.M., Gagnon, A., LaVigne, M., Field, M.P., McDonough, W.F.,
624        2011. Seawater nutrient and carbonate ion concentrations recorded as P/Ca, Ba/Ca,
625        and U/Ca in the deep-sea coral Desmophyllum dianthus. Geochim. Cosmochim. Acta
626        75, 2529–2543. https://doi.org/10.1016/j.gca.2011.02.019

627    Barker, S., Greaves, M., Elderfield, H., 2003. A study of cleaning procedures used for
628        foraminiferal Mg/Ca paleothermometry. Geochemistry, Geophys. Geosystems 4, 8407.
629        https://doi.org/10.1029/2003GC000559

630    Bates, S.L., Hendry, K.R., Pryer, H. V., Kinsley, C.W., Pyle, K.M., Woodward, E.M.S.,
631        Horner, T.J., 2017. Barium isotopes reveal role of ocean circulation on barium cycling in
632        the Atlantic. Geochim. Cosmochim. Acta 204, 286–299.
633        https://doi.org/10.1016/J.GCA.2017.01.043

634    Bice, K.L., Layne, G.D., Dahl, K., 2005. Application of secondary ion mass spectrometry to
635        the determination of Mg/Ca in rare, delicate, or altered planktonic foraminifera:
636        Examples from the Holocene, Paleogene, and Cretaceous. Geochemistry, Geophys.
637        Geosystems 6, Q12P07. https://doi.org/10.1029/2005GC000974

638    Bishop, J.K.B., 1988. The barite-opal-organic carbon association in oceanic particulate
639        matter. Nature 332, 341–343. https://doi.org/10.1038/332341a0

640    Bostock, H.C., Mikaloff Fletcher, S.E., Williams, M.J.M., 2013. Estimating carbonate
641        parameters from hydrographic data for the intermediate and deep waters of the
642        Southern Hemisphere oceans. Biogeosciences 10, 6199–6213.
643        https://doi.org/10.5194/bg-10-6199-2013

644    Bower, A., Furey, H., 2017. Iceland-Scotland Overflow Water transport variability through the
645        Charlie-Gibbs Fracture Zone and the impact of the North Atlantic Current. J. Geophys.
646        Res. Ocean. 122, 6989–7012. https://doi.org/10.1002/2017JC012698

647    Burke, A., Robinson, L.F., 2012. The Southern Ocean's Role in Carbon Exchange During
648        the Last Deglaciation. Science. 335, 557–561. https://doi.org/10.1126/science.1208163

649    Burke, A., Robinson, L.F., McNichol, A.P., Jenkins, W.J., Scanlon, K.M., Gerlach, D.S.,
650        2010. Reconnaissance dating: A new radiocarbon method applied to assessing the
651        temporal distribution of Southern Ocean deep-sea corals. Deep. Res. Part I Oceanogr.
652        Res. Pap. 57, 1510–1520. https://doi.org/10.1016/j.dsr.2010.07.010

653    Cairns, S.D., Kitahara, M. V., 2012. An illustrated key to the genera and subgenera of the

654      Recent azooxanthellate Scleractinia (Cnidaria, Anthozoa), with an attached glossary.

655      Zookeys 227, 1–47. https://doi.org/10.3897/zookeys.227.3612

656 Cantrell, C.A., 2008. Technical Note: Review of methods for linear least-squares fitting of

657      data and application to atmospheric chemistry problems. Atmos. Chem. Phys. Atmos.

658      Chem. Phys. 8, 5477–5487. https://doi.org/10.5194/acpd-8-6409-2008

659 Cardinal, D., Savoye, N., Trull, T.W., André, L., Kopczynska, E.E., Dehairs, F., 2005.

660      Variations of carbon remineralisation in the Southern Ocean illustrated by the Baxs

661      proxy. Deep. Res. Part I Oceanogr. Res. Pap. 52, 355–370.

662      https://doi.org/10.1016/j.dsr.2004.10.002

663 Carritt, D.E., Carpenter, J.H., 1966. Comparison and evaluation of currently employed

664      modifications of the Winkler method for determining dissolved oxygen in sea water. A

665      NASCO Report. J. Mar. Res. 24, 286–318.

666 Case, D.H., Robinson, L.F., Auro, M.E., Gagnon, A.C., 2010. Environmental and biological

667      controls on Mg and Li in deep-sea scleractinian corals. Earth Planet. Sci. Lett. 300,

668      215–225. https://doi.org/10.1016/j.epsl.2010.09.029

669 Chan, L.H., Drummond, D., Edmond, J.M., Grant, B., 1977. On the barium data from the

670      Atlantic GEOSECS expedition. Deep. Res. 24, 613–649. https://doi.org/10.1016/0146-

671      6291(77)90505-7

672 Chen, T.Y., Robinson, L.F., Burke, A., Southon, J., Spooner, P., Morris, P.J., Ng, H.C., 2015.

673      Synchronous centennial abrupt events in the ocean and atmosphere during the last

674      deglaciation. Science. 349, 1537–1541. https://doi.org/10.1126/science.aac6159

675 Cheng, H., Adkins, J., Edwards, L.R., Boyle, E.A., 2000. U-Th dating of deep-sea corals.

676      Geochim. Cosmochim. Acta 64, 2401–2416. https://doi.org/10.1016/S0016-

677      7037(99)00422-6

678 Cohen, A.L., McConnaughey, T.A., 2003. Geochemical perspectives on coral mineralization.

679      Rev. Mineral. Geochemistry 54, 151–187. https://doi.org/10.2113/0540151

680 Collier, R., Edmond, J., 1984. The trace element geochemistry of marine biogenic particulate

681      matter. Prog. Oceanogr. 13, 113–199. https://doi.org/10.1016/0079-6611(84)90008-9

682 Dehairs, F., Chesselet, R., Jedwab, J., 1980. Discrete suspended particles of barite and the

683      barium cycle in the open ocean. Earth Planet. Sci. Lett. 49, 528–550.

684      https://doi.org/10.1016/0012-821X(80)90094-1

685 Dietzel, M., Gussone, N., Eisenhauer, A., 2004. Co-precipitation of $Sr^{2+}$ and $Ba^{2+}$ with

686       aragonite by membrane diffusion of CO2 between 10 and 50 oC. Chem. Geol. 203,

687       139–151. https://doi.org/10.1016/j.chemgeo.2003.09.008

688   Dymond, J., Suess, E., Lyle, M., 1992. Barium in Deep-Sea Sediment: A Geochemical Proxy

689       for Paleoproductivity. Paleoceanography 7, 163–181.

690       https://doi.org/10.1029/92PA00181

691   Gaetani, G.A., Cohen, A.L., 2006. Element partitioning during precipitation of aragonite from

692       seawater: A framework for understanding paleoproxies. Geochim. Cosmochim. Acta

693       70, 4617–4634. https://doi.org/10.1016/j.gca.2006.07.008

694   Gaetani, G.A., Cohen, A.L., Wang, Z., Crusius, J., 2011. Rayleigh-based, multi-element

695       coral thermometry: A biomineralization approach to developing climate proxies.

696       Geochim. Cosmochim. Acta 75, 1920–1932. https://doi.org/10.1016/j.gca.2011.01.010

697   Gagnon, A.C., Adkins, J.F., Fernandez, D.P., Robinson, L.F., 2007. Sr/Ca and Mg/Ca vital

698       effects correlated with skeletal architecture in a scleractinian deep-sea coral and the

699       role of Rayleigh fractionation. Earth Planet. Sci. Lett. 261, 280–295.

700       https://doi.org/10.1016/j.epsl.2007.07.013

701   Ganeshram, R.S., François, R., Commeau, J., Brown-Leger, S.L., 2003. An experimental

702       investigation of barite formation in seawater. Geochim. Cosmochim. Acta 67, 2599–

703       2605. https://doi.org/10.1016/S0016-7037(03)00164-9

704   Gonneea, M.E., Cohen, A.L., DeCarlo, T.M., Charette, M.A., 2017. Relationship between

705       water and aragonite barium concentrations in aquaria reared juvenile corals. Geochim.

706       Cosmochim. Acta 209, 123–134. https://doi.org/10.1016/j.gca.2017.04.006

707   Hathorne, E.C., Gagnon, A., Felis, T., Adkins, J., Asami, R., Boer, W., Caillon, N., Case, D.,

708       Cobb, K.M., Douville, E., Demenocal, P., Eisenhauer, A., Garbe-Schönberg, D.,

709       Geibert, W., Goldstein, S., Hughen, K., Inoue, M., Kawahata, H., Kölling, M., Cornec,

710       F.L., Linsley, B.K., McGregor, H. V., Montagna, P., Nurhati, I.S., Quinn, T.M., Raddatz,

711       J., Rebaubier, H., Robinson, L., Sadekov, A., Sherrell, R., Sinclair, D., Tudhope, A.W.,

712       Wei, G., Wong, H., Wu, H.C., You, C.F., 2013. Interlaboratory study for coral Sr/Ca and

713       other element/Ca ratio measurements. Geochemistry, Geophys. Geosystems 14,

714       3730–3750. https://doi.org/10.1002/ggge.20230

715   Hemsing, F., Hsieh, Y.-T., Bridgestock, L., Spooner, P.T., Robinson, L.F., Frank, N.,

716       Henderson, G.M., 2018. Barium isotopes in cold-water corals. Earth Planet. Sci. Lett.

717       491, 183–192. https://doi.org/10.1016/J.EPSL.2018.03.040

718   Hendry, K.R., Georg, R.B., Rickaby, R.E.M., Robinson, L.F., Halliday, A.N., 2010. Deep

719    ocean nutrients during the Last Glacial Maximum deduced from sponge silicon isotopic

720    compositions. Earth Planet. Sci. Lett. 292, 290–300.

721    https://doi.org/10.1016/j.epsl.2010.02.005

722  Holcomb, M., DeCarlo, T.M., Schoepf, V., Dissard, D., Tanaka, K., McCulloch, M., 2015.

723    Cleaning and pre-treatment procedures for biogenic and synthetic calcium carbonate

724    powders for determination of elemental and boron isotopic compositions. Chem. Geol.

725    398, 11–21. https://doi.org/10.1016/j.chemgeo.2015.01.019

726  Hönisch, B., Allen, K.A., Russell, A.D., Eggins, S.M., Bijma, J., Spero, H.J., Lea, D.W., Yu,

727    J., 2011. Planktic foraminifers as recorders of seawater Ba/Ca. Mar. Micropaleontol. 79,

728    52–57. https://doi.org/10.1016/j.marmicro.2011.01.003

729  Hoppema, M., Dehairs, F., Navez, J., Monnin, C., Jeandel, C., Fahrbach, E., de Baar,

730    H.J.W., 2010. Distribution of barium in the Weddell Gyre: Impact of circulation and

731    biogeochemical processes. Mar. Chem. 122, 118–129.

732    https://doi.org/10.1016/j.marchem.2010.07.005

733  Jacquet, S.H.M., Dehairs, F., Elskens, M., Savoye, N., Cardinal, D., 2007. Barium cycling

734    along WOCE SR3 line in the Southern Ocean. Mar. Chem. 106, 33–45.

735    https://doi.org/10.1016/j.marchem.2006.06.007

736  Jacquet, S.H.M., Dehairs, F., Savoye, N., Obernosterer, I., Christaki, U., Monnin, C.,

737    Cardinal, D., 2008. Mesopelagic organic carbon remineralization in the Kerguelen

738    Plateau region tracked by biogenic particulate Ba. Deep. Res. Part II Top. Stud.

739    Oceanogr. 55, 868–879. https://doi.org/10.1016/j.dsr2.2007.12.038

740  Jeandel, C., Dupre, B., Lebaron, G., Monnin, C., Minster, J.F., 1996. Longitudinal

741    distributions of dissolved barium, silica and alkalinity in the western and southern Indian

742    Ocean. Deep. Res. Part I Oceanogr. Res. Pap. 43, 1–31. https://doi.org/10.1016/0967-

743    0637(95)00098-4

744  Jones, S.M., Murton, B.J., Fitton, J.G., White, N.J., Maclennan, J., Walters, R.L., 2014. A

745    joint geochemical-geophysical record of time-dependent mantle convection south of

746    Iceland. Earth Planet. Sci. Lett. 386, 86–97. https://doi.org/10.1016/j.epsl.2013.09.029

747  LaVigne, M., Grottoli, A.G., Palardy, J.E., Sherrell, R.M., 2016. Multi-colony calibrations of

748    coral Ba/Ca with a contemporaneous in situ seawater barium record. Geochim.

749    Cosmochim. Acta 179, 203–216. https://doi.org/10.1016/j.gca.2015.12.038

750  LaVigne, M., Hill, T.M., Spero, H.J., Guilderson, T.P., 2011. Bamboo coral Ba/Ca:

751    Calibration of a new deep ocean refractory nutrient proxy. Earth Planet. Sci. Lett. 312,

752    506–515. https://doi.org/10.1016/j.epsl.2011.10.013

753    Lea, D.W., Boyle, E.A., 1993. Determination of carbonate-bound barium in foraminifera and

754        corals by isotope dilution plasma-mass spectrometry. Chem. Geol. 103, 73–84.

755        https://doi.org/10.1016/0009-2541(93)90292-Q

756    Lea, D.W., Pak, D.K., Paradis, G., 2005. Influence of volcanic shards on foraminiferal Mg/Ca

757        in a core from the Galápagos region. Geochemistry, Geophys. Geosystems 6, Q11P04.

758        https://doi.org/10.1029/2005GC000970

759    Levitus, S., Boyer, T.P., 1994. World Ocean Atlas 1994 Vol. 4: Temperature, Number 4.

760    Limbeck, A., Galler, P., Bonta, M., Bauer, G., Nischkauer, W., Vanhaecke, F., 2015. Recent

761        advances in quantitative LA-ICP-MS analysis: challenges and solutions in the life

762        sciences and environmental chemistry. Anal. Bioanal. Chem. 407, 6593–6617.

763        https://doi.org/10.1007/s00216-015-8858-0

764    Margolin, A.R., Robinson, L.F., Burke, A., Waller, R.G., Scanlon, K.M., Roberts, M.L., Auro,

765        M.E., van de Flierdt, T., 2014. Temporal and spatial distributions of cold-water corals in

766        the Drake Passage: Insights from the last 35,000 years. Deep. Res. Part II Top. Stud.

767        Oceanogr. 99, 237–248. https://doi.org/10.1016/j.dsr2.2013.06.008

768    McConnaughey, T., 1989. 13C and 18O isotopic disequilibrium in biological carbonates: I.

769        Patterns. Geochim. Cosmochim. Acta 53, 151–162. https://doi.org/10.1016/0016-

770        7037(89)90282-2

771    Mitsuguchi, T., Uchida, T., Matsumoto, E., Isdale, P.J., Kawana, T., 2001. Variations in

772        Mg/Ca, and Sr/Ca ratios of coral skeletons with chemical treatments: Implications for

773        carbonate geochemistry. Geochim. Cosmochim. Acta 65, 2865–2874.

774        https://doi.org/10.1016/S0016-7037(01)00626-3

775    Montagna, P., McCulloch, M., Douville, E., Lopez Correa, M., Trotter, J., Rodolfo-Metalpa,

776        R., Dissard, D., Ferrier-Pages, C., Frank, N., Freiwald, A., Goldstein, S., Mazzoli, C.,

777        Reynaud, S., Ruggeberg, A., Russo, S., Taviani, M., 2014. Li/Mg systematics in

778        scleractinian corals: Calibration of the thermometer. Geochim. Cosmochim. Acta 132,

779        288–310. https://doi.org/10.1016/j.gca.2014.02.005

780    Ni, Y., Foster, G.L., Bailey, T., Elliott, T., Schmidt, D.N., Pearson, P., Haley, B., Coath, C.,

781        2007. A core top assessment of proxies for the ocean carbonate system in surface-

782        dwelling foraminifers. Paleoceanography 22, PA3212.

783        https://doi.org/10.1029/2006PA001337

784 Nozaki, Y., 1997. A fresh look at element distribution in the North Pacific Ocean. Eos, Trans.
785     Am. Geophys. Union 78, 221–221. https://doi.org/10.1029/97EO00148

786 Okai, T., Suzuki, A., Kawahata, H., Terashima, S., Imai, N., 2002. Preparation of a new
787     Geological Survey of Japan geochemical reference material: Coral JCp-1. Geostand.
788     Newsl. 26, 95–99. https://doi.org/10.1111/j.1751-908X.2002.tb00627.x

789 Pierrot, D., Lewis, E., Wallace, D.W.R., 2006. MS Excel program developed for CO2 system
790     calculations. ORNL/CDIAC-105a. Carbon Dioxide Inf. Anal. Center, Oak Ridge Natl.
791     Lab. US Dep. Energy, Oak Ridge, Tennessee.
792     https://doi.org/10.3334/CDIAC/otg.CO2SYS_XLS_CDIAC105a

793 Rae, J.W.B., Foster, G.L., Schmidt, D.N., Elliott, T., 2011. Boron isotopes and B/Ca in
794     benthic foraminifera: Proxies for the deep ocean carbonate system. Earth Planet. Sci.
795     Lett. 302, 403–413. https://doi.org/10.1016/j.epsl.2010.12.034

796 Roberts, J.M., 2006. Reefs of the Deep: The Biology and Geology of Cold-Water Coral
797     Ecosystems. Science. 312, 543–547. https://doi.org/10.1126/science.1119861

798 Robinson, L.F., 2014. RRS James Cook Cruise JC094, October 13–November 30 2013,
799     Tenerife-Trinidad. TROPICS, Tracing Oceanic Processes using Corals and Sediments.
800     Reconstructing abrupt Changes in Chemistry and Circulation of the Equatorial Atlantic
801     Ocean.

802 Robinson, L.F., Adkins, J.F., Frank, N., Gagnon, A.C., Prouty, N.G., Brendan Roark, E., de
803     Flierdt, T. van, 2014. The geochemistry of deep-sea coral skeletons: A review of vital
804     effects and applications for palaeoceanography. Deep. Res. Part II Top. Stud.
805     Oceanogr. 99, 184–198. https://doi.org/10.1016/j.dsr2.2013.06.005

806 Rosenthal, Y., Field, M.P., Sherrell, R.M., 1999. Precise determination of element/calcium
807     ratios in calcareous samples using sector field inductively coupled plasma mass
808     spectrometry. Anal. Chem. 71, 3248–3253. https://doi.org/10.1021/ac981410x

809 Rosenthal, Y., Perron-Cashman, S., Lear, C.H., Bard, E., Barker, S., Billups, K., Bryan, M.,
810     Delaney, M.L., DeMenocal, P.B., Dwyer, G.S., Elderfield, H., German, C.R., Greaves,
811     M., Lea, D.W., Marchitto, T.M., Pak, D.K., Paradis, G.L., Russell, A.D., Schneider, R.R.,
812     Scheiderich, K., Stott, L., Tachikawa, K., Tappa, E., Thunell, R., Wara, M., Weldeab, S.,
813     Wilson, P.A., 2004. Interlaboratory comparison study of Mg/Ca and Sr/Ca
814     measurements in planktonic foraminifera for paleoceanographic research.
815     Geochemistry, Geophys. Geosystems 5, Q04D09.
816     https://doi.org/10.1029/2003GC000650

817  Shen, G.T., Boyle, E.A., 1988. Determination of lead, cadmium and other trace metals in
818      annually-banded corals. Chem. Geol. 67, 47–62. https://doi.org/10.1016/0009-
819      2541(88)90005-8

820  Sinclair, D.J., Williams, B., Risk, M., 2006. A biological origin for climate signals in corals -
821      Trace element "vital effects" are ubiquitous in Scleractinian coral skeletons. Geophys.
822      Res. Lett. 33, L17707. https://doi.org/10.1029/2006GL027183

823  Spooner, P.T., Chen, T., Robinson, L.F., Coath, C.D., 2016a. Rapid uranium-series age
824      screening of carbonates by laser ablation mass spectrometry. Quat. Geochronol. 31,
825      28–39. https://doi.org/10.1016/j.quageo.2015.10.004

826  Spooner, P.T., Guo, W., Robinson, L.F., Thiagarajan, N., Hendry, K.R., Rosenheim, B.E.,
827      Leng, M.J., 2016b. Clumped isotope composition of cold-water corals: A role for vital
828      effects? Geochim. Cosmochim. Acta 179, 123–141.
829      https://doi.org/10.1016/j.gca.2016.01.023

830  Sternberg, E., Tang, D., Ho, T.Y., Jeandel, C., Morel, F.M.M., 2005. Barium uptake and
831      adsorption in diatoms. Geochim. Cosmochim. Acta 69, 2745–2752.
832      https://doi.org/10.1016/j.gca.2004.11.026

833  Stroobants, N., Dehairs, F., Goeyens, L., Vanderheijden, N., Van Grieken, R., 1991. Barite
834      formation in the Southern Ocean water column. Mar. Chem. 35, 411–421.
835      https://doi.org/10.1016/S0304-4203(09)90033-0

836  Sundby, S., Drinkwater, K.F., Kjesbu, O.S., 2016. The North Atlantic Spring-Bloom
837      System—Where the Changing Climate Meets the Winter Dark. Front. Mar. Sci. 3, 28.
838      https://doi.org/10.3389/fmars.2016.00028

839  Thiagarajan, N., Subhas, A. V., Southon, J.R., Eiler, J.M., Adkins, J.F., 2014. Abrupt pre-
840      Bølling–Allerød warming and circulation changes in the deep ocean. Nature 511, 75–
841      78. https://doi.org/10.1038/nature13472

842  Tudhope, A.W., Lea, D.W., Shimmield, G.B., Chilcott, C.P., Head, S., 1996. Monsoon
843      climate and Arabian sea Coastal Upwelling Recorded in Massive Corals from Southern
844      Oman. Palaios 11, 347–361. https://doi.org/10.2307/3515245

845  van Beek, P., Sternberg, E., Reyss, J.L., Souhaut, M., Robin, E., Jeandel, C., 2009.
846      228Ra/226Ra and 226Ra/Ba ratios in the Western Mediterranean Sea: Barite formation
847      and transport in the water column. Geochim. Cosmochim. Acta 73, 4720–4737.
848      https://doi.org/10.1016/j.gca.2009.05.063

849 van de Flierdt, T., Robinson, L.F., Adkins, J.F., 2010. Deep-sea coral aragonite as a

850     recorder for the neodymium isotopic composition of seawater. Geochim. Cosmochim.

851     Acta 74, 6014–6032. https://doi.org/10.1016/j.gca.2010.08.001

852 Watanabe, T., Minagawa, M., Oba, T., Winter, A., 2001. Pretreatment of coral aragonite for

853     Mg and Sr analysis: Implications for coral thermometers. Geochem. J. 35, 265–269.

854     https://doi.org/10.2343/geochemj.35.265

855 York, D., Evensen, N.M., Martínez, M.L., De Basabe Delgado, J., 2004. Unified equations for

856     the slope, intercept, and standard errors of the best straight line. Am. J. Phys. 72, 367.

857     https://doi.org/10.1119/1.1632486

858

| Cleaning step | Fe/Ca (µmol/mol) | Err. (2 S.E.) | Ba/Ca (µmol/mol) | Err. (2 S. E.) |
|---|---|---|---|---|
| NBP0805-TB10-Dp-3 | | | | |
| 2 | 2.05 | 0.07 | 12.46 | 0.13 |
| 3 | 1.67 | 0.06 | 12.62 | 0.13 |
| 4 | 1.26 | 0.04 | 12.30 | 0.13 |
| 5 | 0.89 | 0.03 | 12.36 | 0.13 |
| 6 | 1.99 | 0.07 | 12.67 | 0.13 |
| 7 | 1.00 | 0.03 | 12.38 | 0.13 |
| CE0806-Dr18-1 | | | | |
| 1 | 44.05 | 1.45 | 7.33 | 0.08 |
| 2 | 41.92 | 1.38 | 7.35 | 0.08 |
| 4 | 19.6 | 0.65 | 7.18 | 0.08 |
| 6 | 9.15 | 0.3 | 7.21 | 0.08 |
| 7 | 4.26 | 0.14 | 7.20 | 0.08 |

859

860 Table 1: Elemental ratios of corals measured after chemical cleaning. Cleaning steps follow

861 the descriptions in the text: 1) Shipboard washes and lab-based physical cleaning only, 2) 15

862 min US in milli-q and powdering; 3) 15 min US oxidising solution; 4) 2 min perchloric acid

863 rinse; 5) 15 min US in milli-q; 6) 1 min US in 0.2 % $HNO_3$; 7) as 3; 8) 20 min US reducing

864 solution. Every sample was replicated once and the ratios here are the mean of the two
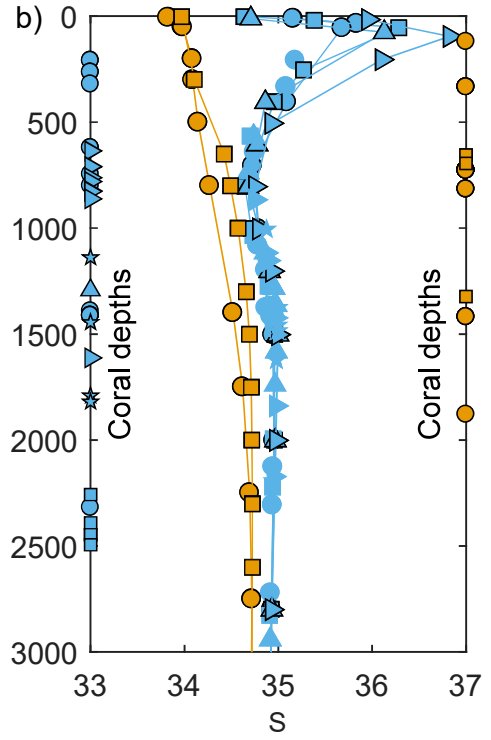
865 replicates of each cleaning stage.

866

**Figure 1**

Septa

Septa

Septa cross section

COC

Pali

Columella

TDs

Theca

Base (unattached)

Pedicel

Base (attached)

**Figure 2**

**Figure 3**

a)

Depth (m) — T (°C)

b)

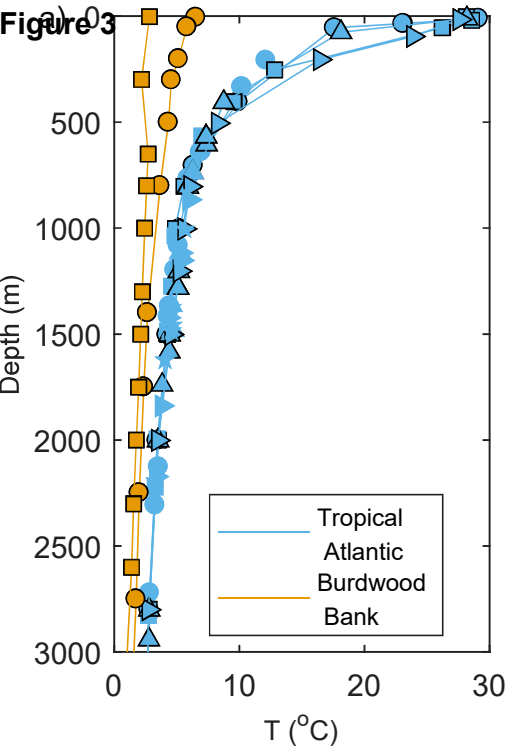S — Coral depths — Coral depths
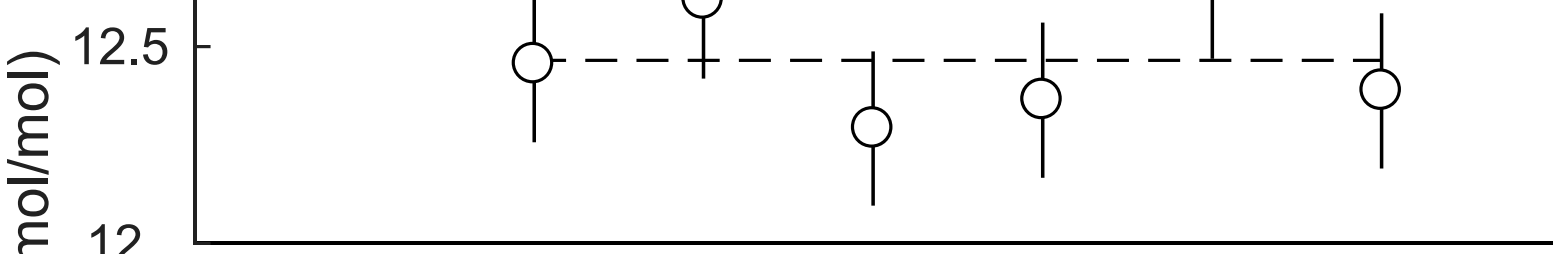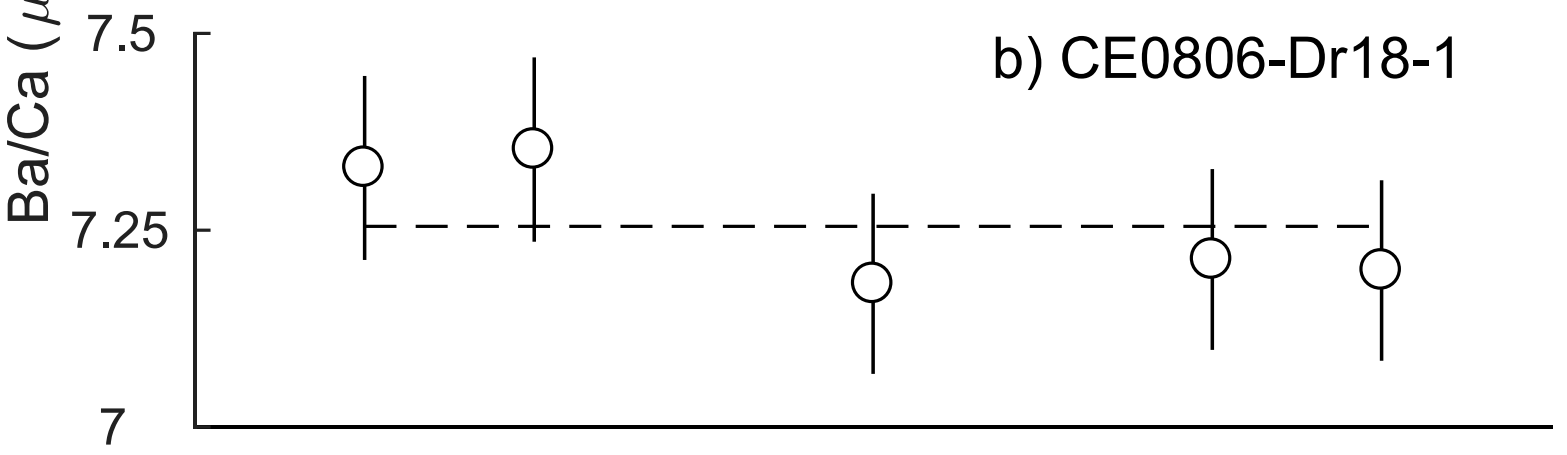
c)

Ba (nmol/kg)

Tropical Atlantic
Burdwood Bank
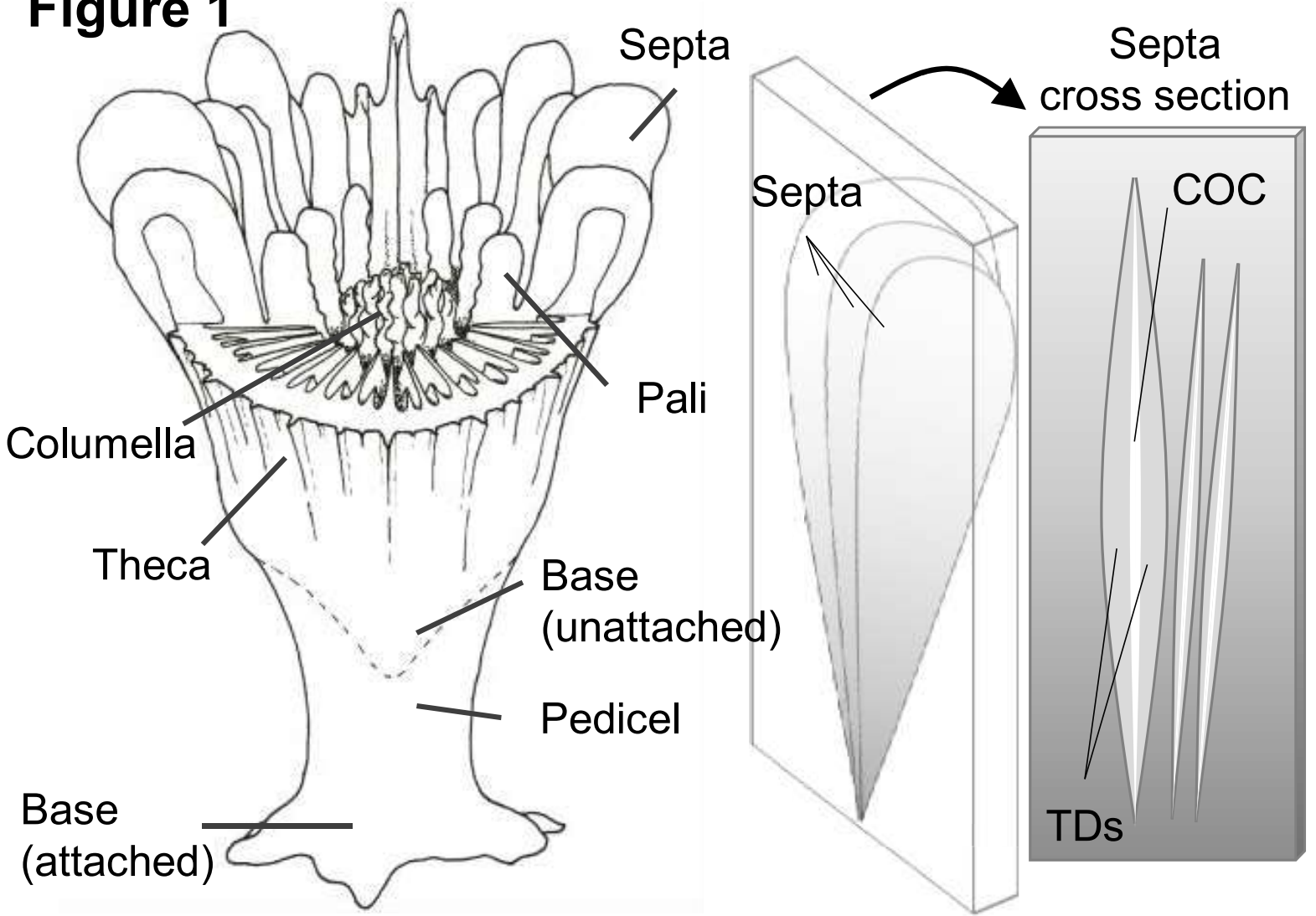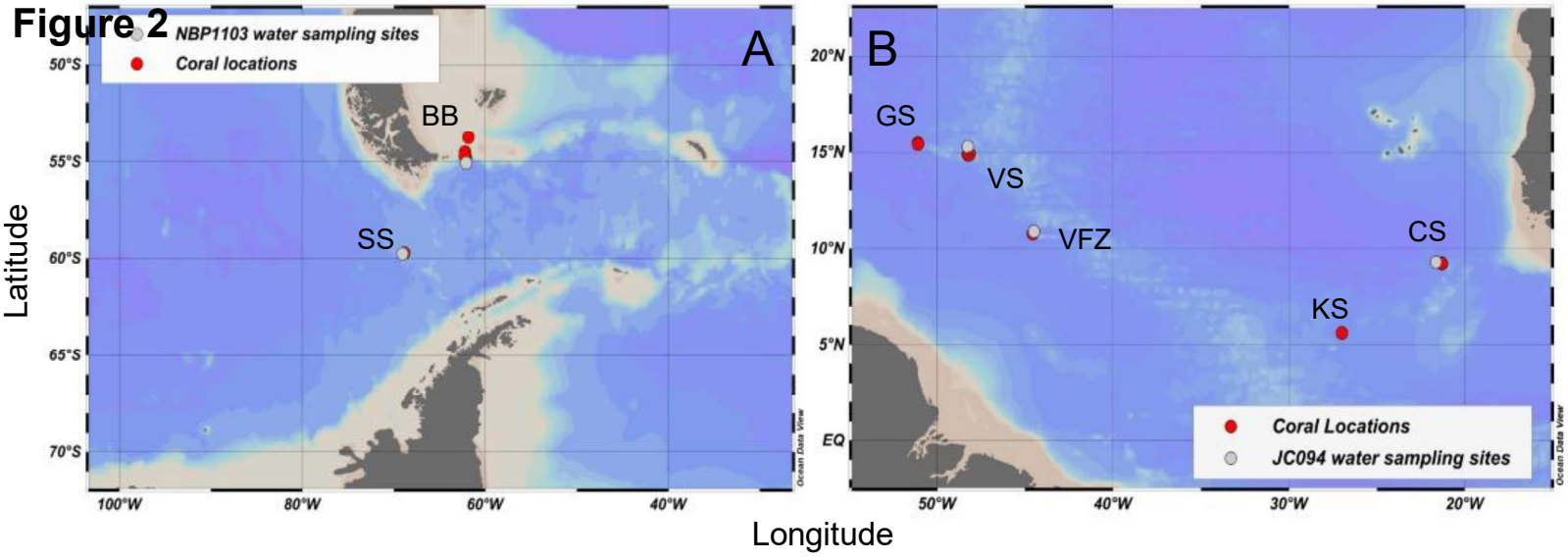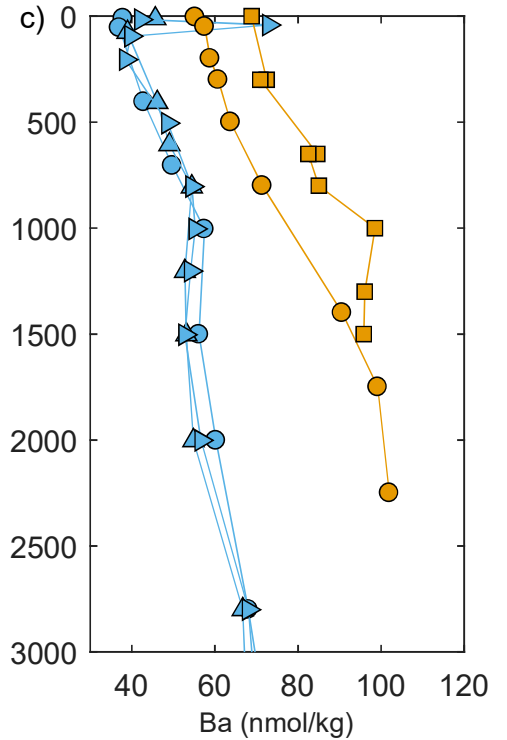
Carter Seamount    Knipovich Seamount    Vema Fracture Zone    Vayda Seamount    Gramberg Seamount
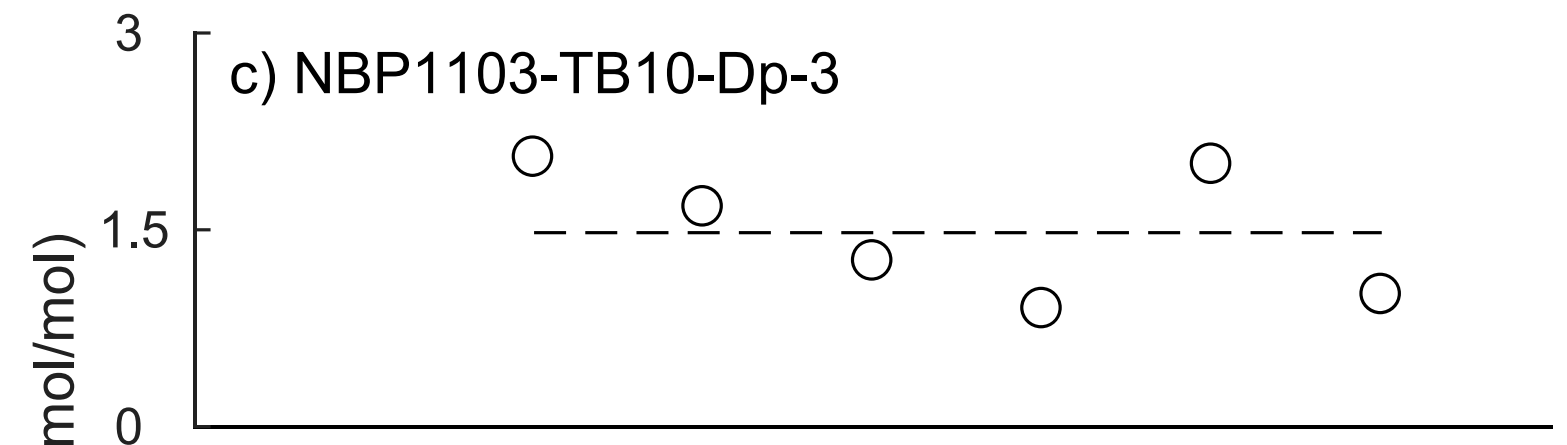
Sars Seamount    Drake Passage

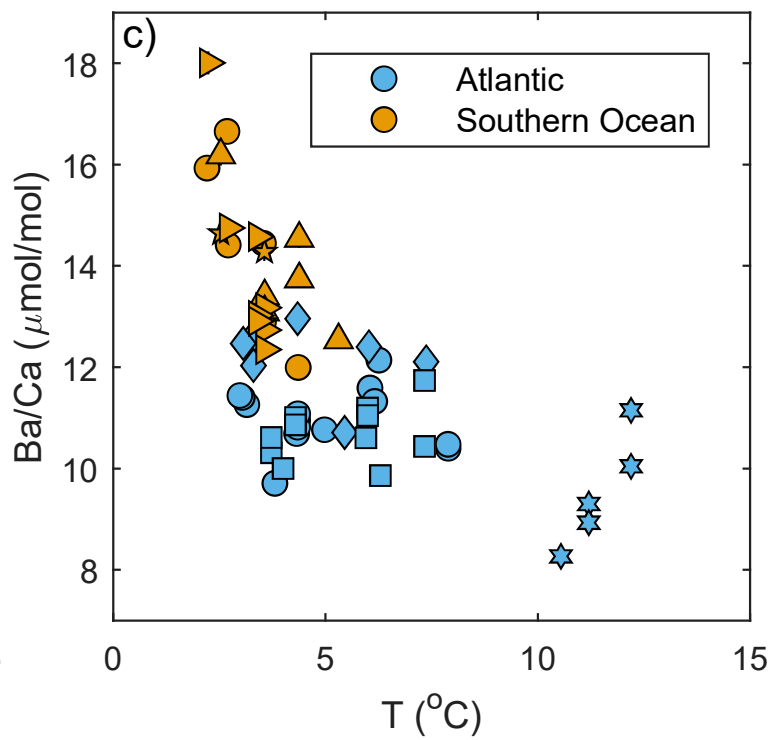**Figure 4**
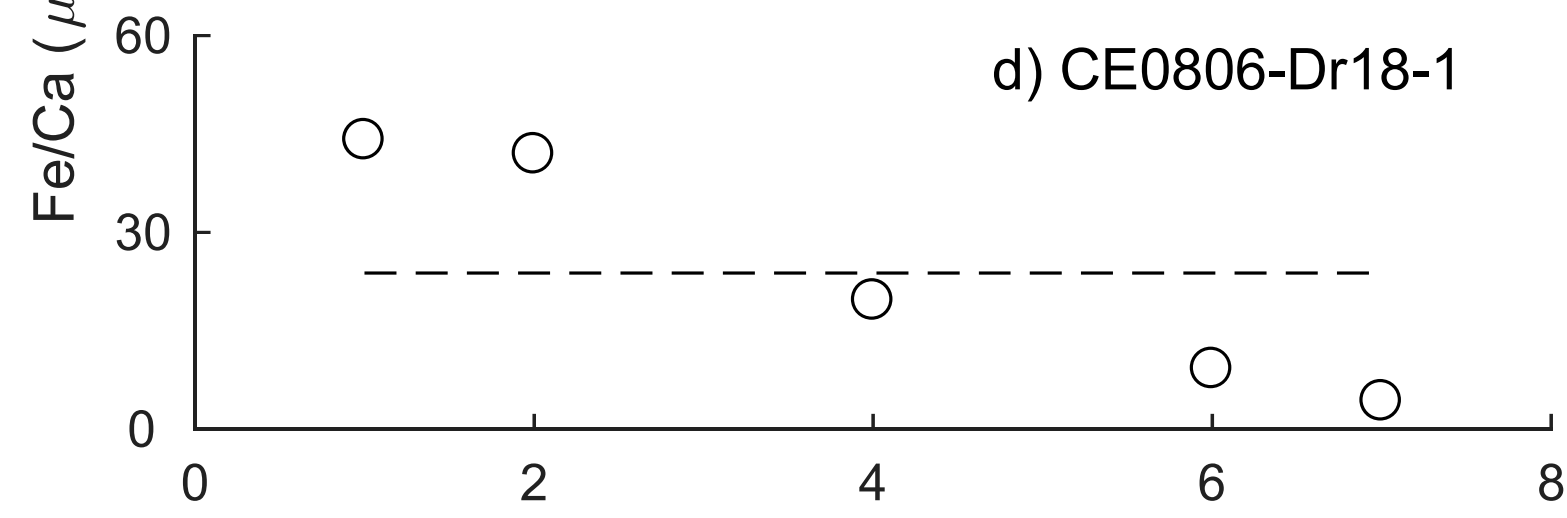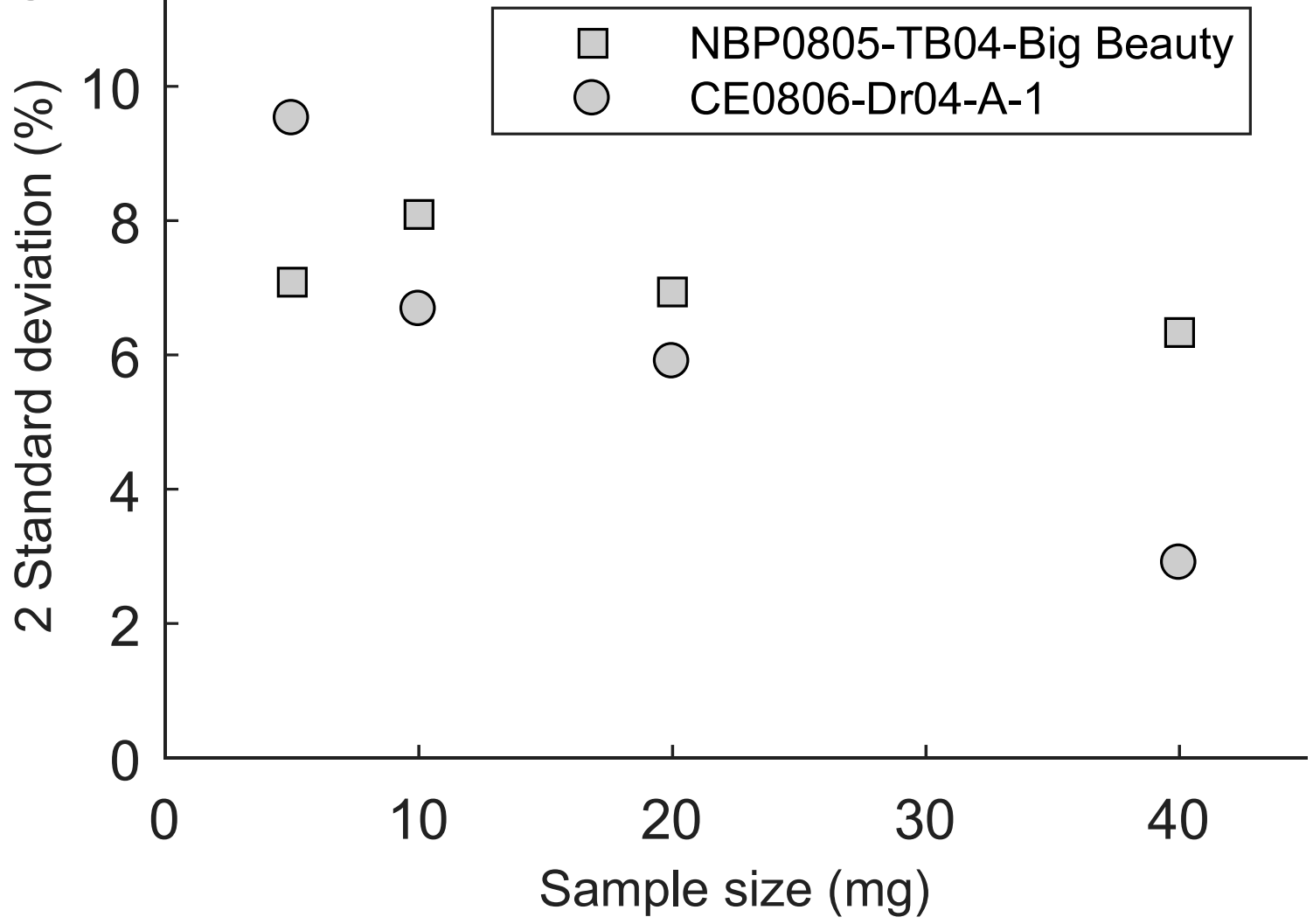
**Figure 5**
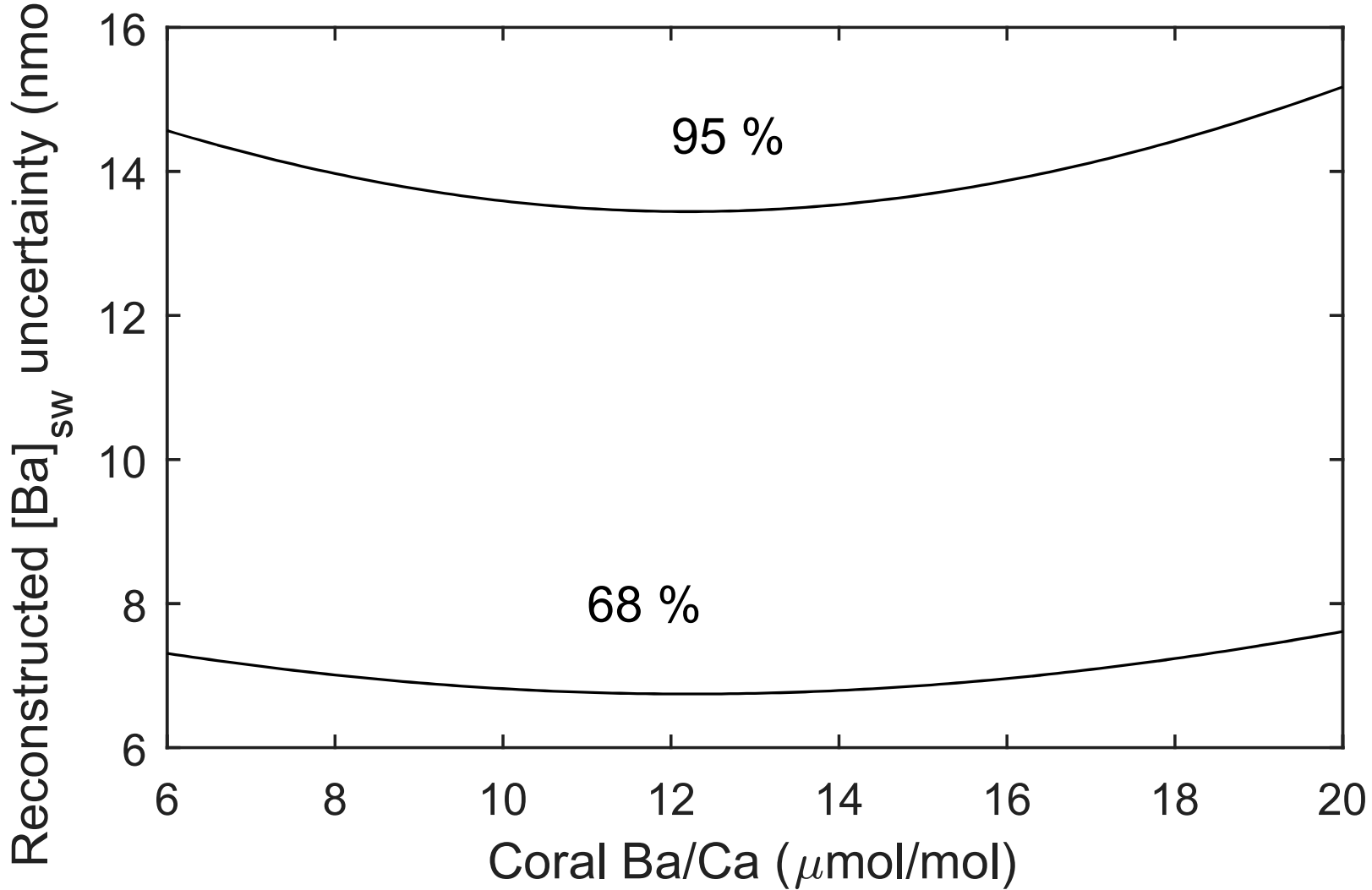
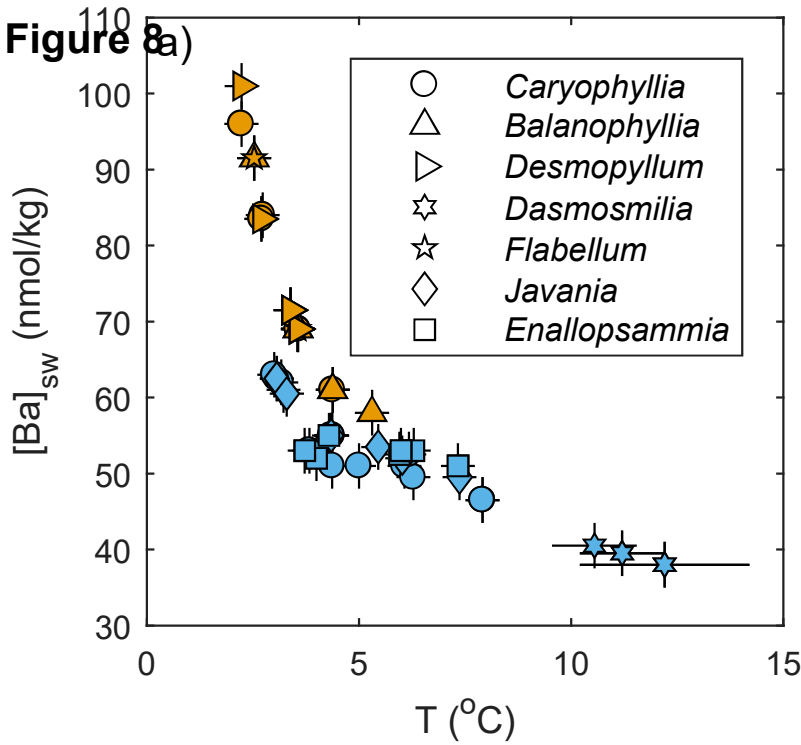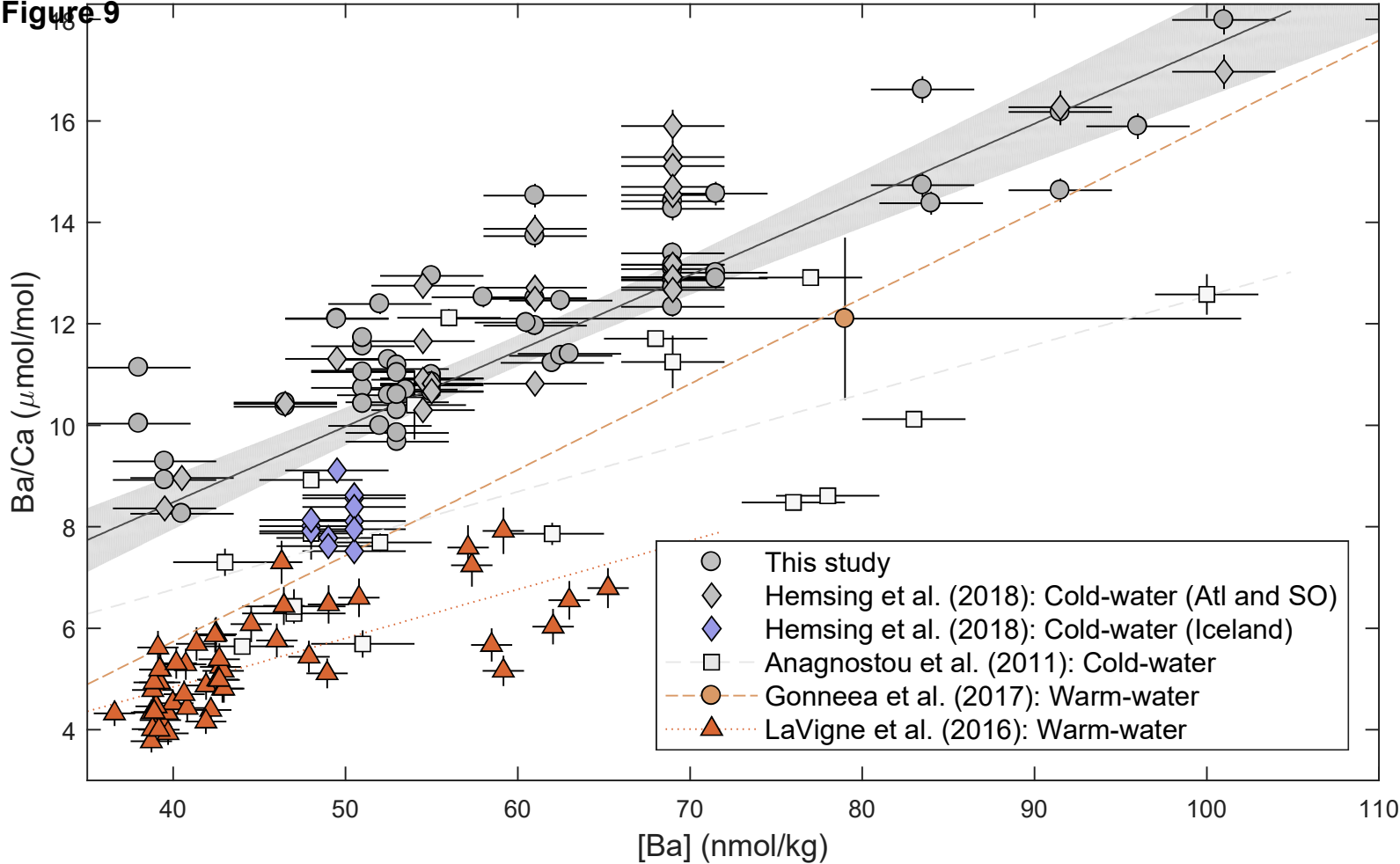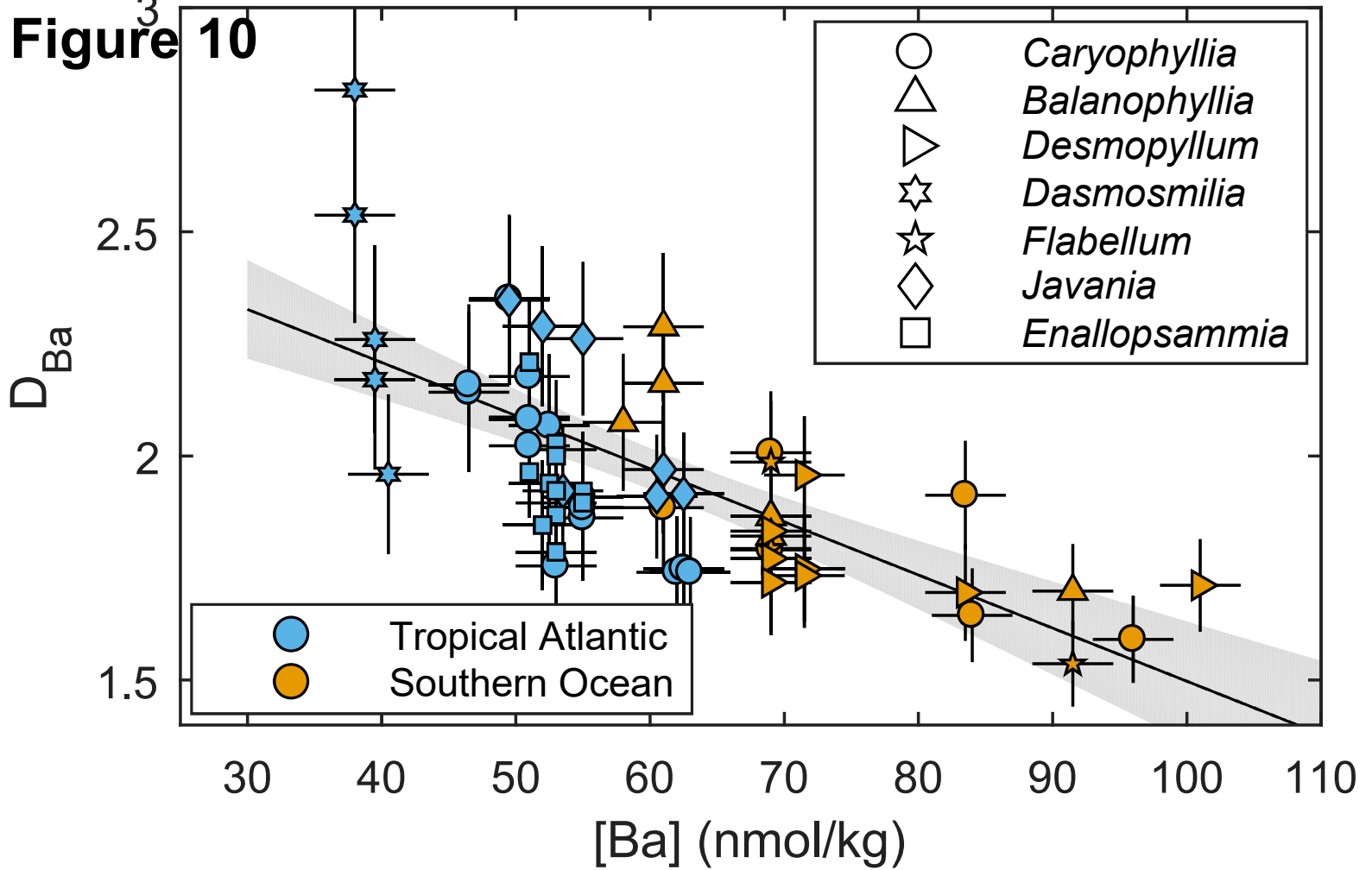**Figure 6**
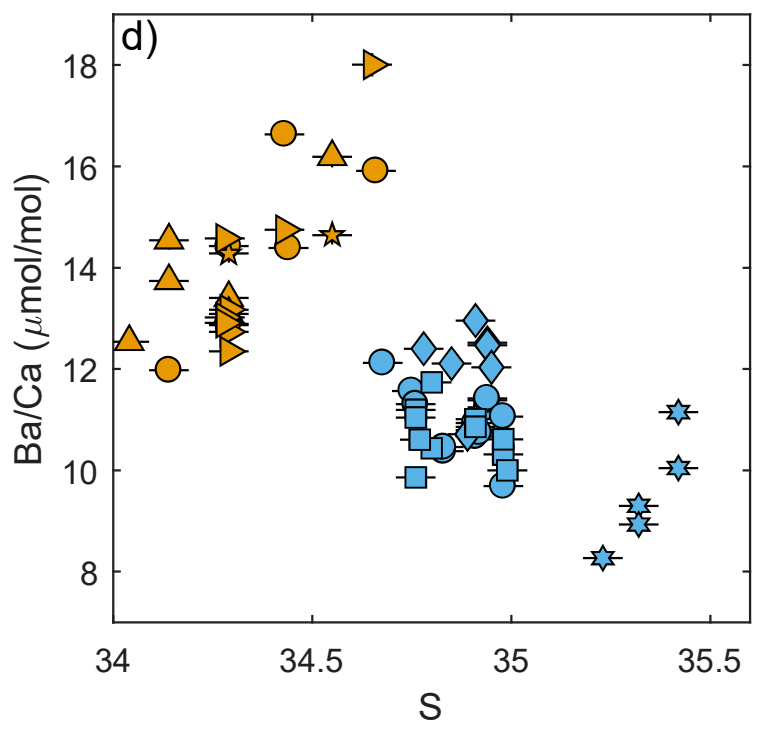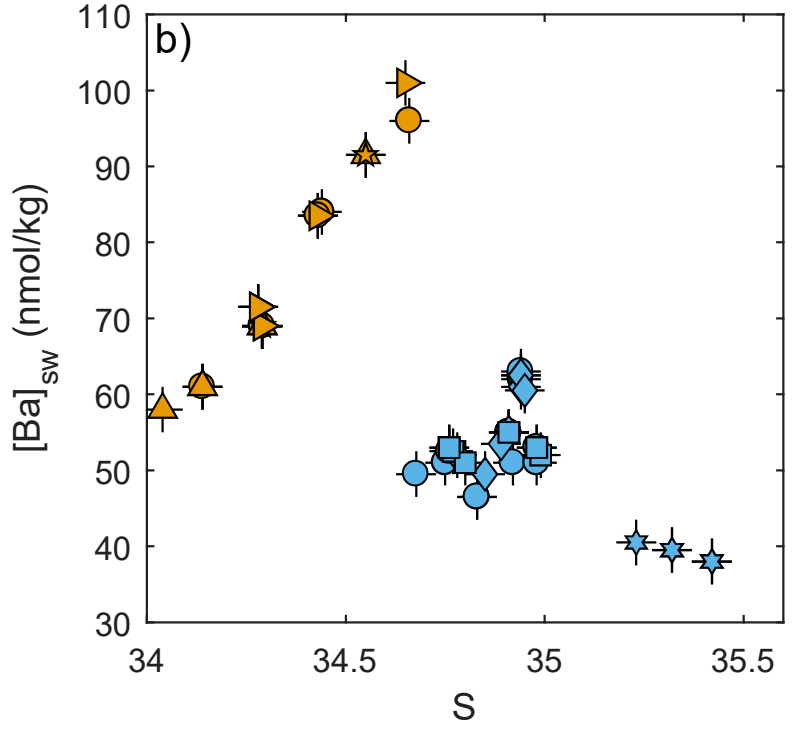
Figure 7

Figure 8

Figure 9

**Figure 10**

Extended calibration of cold-water coral Ba/Ca using multiple genera and co-located measurements of dissolved barium concentration: List of figures

1. Maps of a) Drake Passage and b) tropical Atlantic sample sites. Red points indicate coral collection sites named as follows: a) BB, Burdwood Bank; SS, Sars Seamount; b) GS, Gramberg Seamount; VS, Vayda Seamount; VFZ, Vema Fracture Zone; KS, Knipovich Seamount; CS, Carter Seamount. Grey points indicate locations where $[Ba]_{sw}$ has been measured in seawater samples. Plotted using Ocean Data View.

2. Typical solitary cold-water coral skeleton of the genus Caryophyllia, labelled with the macroscale features and redrawn after Cairns and Kitahara (2012), and a schematic cross section through a coral septum illustrating the microscale features COCs and TDs.

3. Measured a) Temperature, b) Salinity and c) $[Ba]_{sw}$ (nmol/kg) depth profiles near each sample site. Samples from CTD casts are shown with black outline. Samples from Niskin bottles aboard the ROV are shown with no outline. Coral sample depths are shown along the sides of panel (b). Estimates of water properties at the depths of coral collection are based on extrapolation of the data in the relevant curve to that depth. In some cases, temperature and salinity were measured as the corals were collected (Spooner et al. 2016b).

4. Impact of chemical cleaning on the measured Ba/Ca (a,b) and Fe/Ca (c,d) of powders from the corals NBP1103-TB10-Dp-3 (Desmophyllum; a,c) and CE0806-Dr18-1 (Desmophyllum; b,d). Cleaning stages are numbered as follows: 1) shipboard washing and lab-based physical cleaning only, 2) 15 min US in milli-q; 3) 15 min US oxidising solution; 4) 2 min perchloric acid rinse; 5) 15 min US in milli-q; 6) 1 min US in 0.2 % $HNO_3$; 7) as 3; 8) 20 min US reducing solution. Full details of the oxidising and reducing solutions can be found in Section 2.4. Dashed lines indicate the means of the measurements. Where no error bars can be seen, errors are smaller than the data points.

5. 2 standard deviations of Ba/Ca ratios taken from different size fractions for the corals NBP0805-TB04-Big Beauty (10 samples per size fraction) and CE0806-DR04A-1 (5 samples per size fraction).

6. Ba/Ca in coral skeletons versus dissolved seawater Ba concentration ($[Ba]_{sw}$). A linear least squares lines of best fit is drawn through the data (solid line) with confidence intervals (grey area, 2 S.E.) included. The dashed line indicates the weighted bivariate fit as discussed in Section 3.3. Vertical error bars are based on the 2 S.D. of repeat Ba/Ca measurements on the standard materials. Horizontal error bars are estimates of the $[Ba]_{sw}$ uncertainty. Where no vertical error bars can be seen, errors are smaller than the data points.

7. Reconstruction uncertainties on the dissolved seawater Ba concentration ($[Ba]_{sw}$) when estimated from cold-water coral Ba/Ca using the calibration from data in this study. Both the 95 % and 68 % uncertainty intervals are indicated.

8. a) Dissolved Ba in seawater ($[Ba]_{sw}$) versus seawater temperature (T) and b) salinity (S) for the sample sites from which corals were collected during this study. c) Coral skeleton Ba/Ca ratio versus T and d) S for the same sample sites.

9. Measured Ba/Ca in coral skeletons versus dissolved seawater Ba concentration ($[Ba]_{sw}$) in multiple studies. Data from this study and Hemsing et al. (2018) have been corrected as described in the text, and the linear least squares fit through all the data from the two studies (averaged where the same coral was measured in both studies) is shown with confidence intervals. Linear least squares lines of best fit are also shown for the data from each other study individually.

10. Calculated $D_{Ba}$ versus $[Ba]_{sw}$ for the data presented in this study. A linear least squares fit is plotted through the data for illustrative purposes.